THE DOWNSHIFT OF ELECTRON PLASMA OSCILLATIONS IN THE ELECTRON FORESHOCK REGION

by

Stephen A. Fuselier

An Abstract

Of a thesis submitted in partial fulfillment
of the requirements for the Doctor of
Philosophy degree in Physics
in the Graduate College of
The University of Iowa

December 1984

Thesis supervisor: Professor Donald A. Gurnett

ABSTRACT

Electron plasma oscillations in the Earth's electron foreshock region are observed to shift above and below the local electron plasma frequency. As plasma oscillations shift from the plasma frequency, their bandwidth increases and their wavelength decreases. Observations of plasma oscillations well below the plasma frequency are correlated with times when ISEE-1 is far downstream of the electron foreshock boundary. Although wavelengths of plasma oscillations below the plasma frequency satisfy $k\lambda_{De} \approx 1$, the Doppler-shift due to the motion of the solar wind is not sufficient to produce the observed frequency shifts. A beam-plasma interaction with beam velocities on the order of the electron thermal velocity is suggested as an explanation for plasma oscillations above and below the plasma frequency. Frequency, bandwidth, and wavelength changes predicted from the beam-plasma interaction are in good agreement with the observed characteristics of plasma oscillations in the foreshock region.

Abstract approved: Donald A. Gurnett
Thesis supervisor

Professor, Physics and Astronomy
Title and Department

June 27, 1984
Date

THE DOWNSHIFT OF ELECTRON PLASMA OSCILLATIONS IN THE ELECTRON FORESHOCK REGION

by

Stephen A. Fuselier

A thesis submitted in partial fulfillment
of the requirements for the Doctor of
Philosophy degree in Physics
in the Graduate College of
The University of Iowa

December 1984

Thesis supervisor: Professor Donald A. Gurnett

Graduate College
The University of Iowa
Iowa City, Iowa

CERTIFICATE OF APPROVAL

PH.D. THESIS

This is to certify that the Ph.D. thesis of

Stephen A. Fuselier

has been approved by the Examining Committee for the thesis requirement for the Doctor of Philosophy degree in Physics at the December 1984 graduation.

Thesis committee: D. A. Imrett
Thesis supervisor

Member

J. A. Van Allen
Member

L. A. Frank
Member

Member

ACKNOWLEDGEMENTS

I thank Dr. Gurnett for his careful guidance and financial support during the past year. In addition to teaching me the plasma physics I needed to complete this thesis, his support and encouragement helped me overcome the many problems that stem from being a graduate student. I also thank Richard Fitzenreiter for providing all the electron data in this thesis. Through countless telephone conversations and three visits to Goddard, he provided valuable information on the electron spectrometer and the interpretation of the electron data.

I thank Kathy Kurth for typing the many revisions of the paper and thesis. She also arranged transportation and accommodations for all the conferences and meetings I attended this past year. I also thank Chris Joyner for some timely typing while Kathy was on a well deserved "vacation." I am indebted to my wife, Bette, for the proofreading she did. It's nice to have a wife that can correct not only grammar and spelling, but also mathematical derivations. Without Joyce Chrisinger, there would be no figures in this thesis. She suffered through my many revisions and always produced top quality work. Mark Brown did his usual excellent photography work. He provided all the wideband photography in this thesis. Sharon Hanson and Paul Holland processed many hours of wideband data. These data are the central part of

observations in this thesis. Roger Anderson, in addition to his help, allowed me to have free reign when it came to getting wideband data processed. I also thank C. S. Lin of the Southwest Research Institute for providing the routines used to solve the plasma dispersion function and the dispersion relation. Dr. Georg Knorr helped me with the problem of the spacecraft position relative to the tangent field line that is discussed in the appendix.

There are many others (faculty, staff, and graduate students) who have made my graduate career worthwhile. For them, I say thanks, it's been an enjoyable experience.

Finally, I thank my wife Bette for putting up with me. Graduate school is a trying time in a relationship and I think both of us have weathered it well.

This research was supported by contract NAS5-26819 with Goddard Space Flight Center and grant NGL-16-001-043 with NASA Headquarters.

ABSTRACT

Electron plasma oscillations in the Earth's electron foreshock region are observed to shift above and below the local electron plasma frequency. As plasma oscillations shift from the plasma frequency, their bandwidth increases and their wavelength decreases. Observations of plasma oscillations well below the plasma frequency are correlated with times when ISEE-1 is far downstream of the electron foreshock boundary. Although wavelengths of plasma oscillations below the plasma frequency satisfy $k\lambda_{De} \approx 1$, the Doppler-shift due to the motion of the solar wind is not sufficient to produce the observed frequency shifts. A beam-plasma interaction with beam velocities on the order of the electron thermal velocity is suggested as an explanation for plasma oscillations above and below the plasma frequency. Frequency, bandwidth, and wavelength changes predicted from the beam-plasma interaction are in good agreement with the observed characteristics of plasma oscillations in the foreshock region.

TABLE OF CONTENTS

LIST OF FIGURES

I. INTRODUCTION

In this thesis, observations of electron plasma oscillations are interpreted using a beam-plasma theory. Electron plasma oscillations upstream of the Earth's bow shock were first reported by Fredricks et al. [1968]. Using OGO-5 spacecraft data, they reported enhanced electric field intensities near the local electron plasma frequency. Also using OGO-5 spacecraft data, Scarf et al. [1971] identified electric field enhancements near the local plasma frequency and associated these enhancements with electrons streaming from the bow shock. The waves were identified by Scarf et al. as either electron plasma oscillations or upper hybrid waves. Fredricks et al. [1971] demonstrated that observations of electric field enhancements near the plasma frequency were consistent with the interpretation that the waves were electron plasma oscillations generated by a beam-plasma interaction. The electrostatic nature of the waves was confirmed by Rodriguez and Gurnett [1975], using simultaneous electric and magnetic field measurements from IMP-6.

Following the identification of the emissions as electron plasma oscillations, their polarization and wavelength were measured by several investigators. The polarization of the emissions was measured from IMP-6 data by Rodriguez and Gurnett [1975, 1976]. The polarization was found to be primarily along the magnetic field. This measurement confirmed the identification of the waves as electron plasma oscillations,

and eliminated the possibility that they are upper hybrid waves. The wavelength of plasma oscillations was estimated to be several kilometers by Gurnett and Frank [1975]. These wavelength estimates were confirmed by Gurnett et al. [1979] and Anderson et al. [1981], using ISEE-1 and -2 electric field data.

Filbert and Kellogg [1979] considered the characteristics of the beam generated plasma oscillations in more detail. They considered the effect of the motion of the solar wind on electrons streaming from the bow shock. Electrons streaming from the bow shock are convected downstream due to the $\vec{v} \times \vec{B}$ electric field of the solar wind. As illustrated in Figure 1, high energy electrons originating from the tangent point define a boundary called the electron foreshock boundary. Upstream of this boundary, no electrons streaming from the bow shock are observed. The region downstream of the foreshock boundary and upstream of the bow shock is called the electron foreshock region. Filbert and Kellogg noted that electrons streaming into the solar wind from the bow shock with velocities below a certain critical velocity are convected downstream before they reach the spacecraft. The magnitude of the critical velocity depends on the location of the spacecraft in the foreshock region. In the foreshock region, the reduced one dimensional electron distribution in the plasma rest frame has a positive slope at the critical velocity. This reduced electron distribution is called a time-of-flight distribution. Filbert and Kellogg considered a model time-of-flight distribution with the critical velocity much greater than the electron thermal velocity and demonstrated that

plasma oscillations can be generated near the electron plasma frequency. This model is valid for times when the spacecraft is located at the foreshock boundary. Intense electrostatic emissions at the plasma frequency were reported by Filbert and Kellogg coincident with foreshock boundary crossings. They suggested that high energy electron beams, of the type first reported by Anderson [1968, 1969], should be coincident with foreshock boundary crossings. Thin sheets of high energy electrons associated with the foreshock boundary were reported by Anderson et al. [1979].

Plasma oscillations are observed to vary in frequency. Frequency variations of plasma oscillations on the order of a few kHz were reported by Fredricks et al. [1972]. These frequency variations were correlated with fluctuations in both the local electron density and the total magnetic field. Based on the magnetic field fluctuations, it was suggested by Fredricks et al. that these frequency variations were caused by electron density fluctuations associated with oblique magnetohydrodynamic waves in the foreshock region. An example of frequency variations of plasma oscillations is illustrated in Figure 2. Figure 2 is a frequency-time spectrogram from ISEE-1. The local plasma frequency, which varies between 20 and 30 kHz, was calculated from measurements of the electron density. Emissions identified as electron plasma oscillations occur at the local plasma frequency. The presence of ion acoustic waves between 0 and 10 kHz has been correlated with ions streaming from the bow shock [Scarf et al., 1970]. These ions are

believed to provide a source of free energy for generation of magnetohydrodynamic waves [Scarf et al., 1970].

Frequency variations of plasma oscillations were also reported by Rodriquez and Gurnett [1975]. Rodriguez and Gurnett reported observations of electrostatic emissions from 3 kHz to the plasma frequency, which is usually about 30 kHz. It is not clear from their study which electrostatic wave mode was observed below the plasma frequency. The emissions observed could have been a mixture of ion acoustic waves, which range from 0 to 10 kHz, and electron plasma oscillations, which as will be shown, range from near 0 kHz to about 30 kHz. It was suggested by Rodriguez and Gurnett that the emissions below the plasma frequency were plasma oscillations that were strongly Doppler shifted due to the motion of the solar wind. However, their explanation is doubtful because if the wavelength is several kilometers, as estimated by Gurnett and Frank [1975], then the Doppler shift due to the motion of the solar wind is less than 1 kHz.

The purpose of this thesis is to report and interpret new observations of electron plasma oscillations downstream of the electron foreshock. It will be shown that plasma oscillations can be observed at, above, and in some cases substantially below the plasma frequency. The observed frequency shifts are correlated with the spacecraft location in the foreshock region and with variations in the spectrum of electrons arriving from the bow shock. A mechanism for generation of plasma oscillations at all observed frequencies will be suggested. Predic-

tions from the mechanism are found to agree with observations of frequency shift, bandwidth, and wavelength of plasma oscillations.

Plasma wave data from the University of Iowa plasma wave instruments on ISEE-1 and -2 are used in this study. A description of the plasma wave instruments is given by Gurnett et al. [1978]. Density, solar wind velocity, and temperature values in this study are a result of moment calculations of three dimensional distributions measured by the Goddard Space Flight Center electron spectrometer on ISEE-1. For information on the Goddard Space Flight Center electron spectrometer, see Ogilvie et al. [1978]. In addition to moments of the electron distribution, the time evolution of the reduced one dimensional electron distribution, $F(v_{\parallel})$ is used in this study.

II. OBSERVATIONS OF PLASMA OSCILLATIONS

Electron plasma oscillations observed in the electron foreshock region occur at the local plasma frequency, and in some cases may shift slightly above or substantially below the plasma frequency. Plasma oscillations are observed at frequencies ranging from less than 0.1 f_{pe} to about 1.1 f_{pe}. For the foreshock region, this frequency range is from about 3 to 30 kHz. A typical example of plasma oscillations that are shifted substantially from the plasma frequency is illustrated in Figure 3. The upper panel of Figure 3 is a wideband frequency-time spectrogram from the ISEE-1 wideband receiver which was taken when the spacecraft was located in the foreshock region. In the lower panel of Figure 3, the plasma frequency was calculated from the equation $f_{pe} = 9000\sqrt{n_o}$, where n_o is the electron density in units of cm^{-3}, and the frequency is in Hz. During the time interval from 0633 UT to 0633:30 UT, the plasma oscillations are seen to vary from the plasma frequency to about .25 ω_{pe}. There is a difference between frequency shifts of plasma oscillations presented in this paper and frequency variations reported by Fredricks et al. [1972]. The plasma oscillations illustrated in Figure 3 are not always at the plasma frequency, whereas plasma oscillations reported by Fredricks et al. and illustrated in Figure 2 are always at or near the plasma frequency.

Another characteristic of plasma oscillations is illustrated in Figure 3. At 0638:40 UT, the plasma oscillations appear as a narrow-band emission near the plasma frequency. From 0638:40 UT to 0639 UT, the plasma oscillations shift downward from the plasma frequency. Coincident with this shift, the bandwidth of the emissions increases from a few hundred Hz to about ±2 kHz. From the study of numerous events such as those illustrated in Figure 3, it was found that an increase in the bandwidth of plasma oscillations always accompanies a large shift in the frequency away from the plasma frequency.

In addition to the change in the bandwidth, the wavelength of plasma oscillations below the plasma frequency also changes. The wavelength of electrostatic emissions such as plasma oscillations can be infered by comparing spectral density measurements obtained from two different length electric antennas. To obtain the wavelengths of plasma oscillations at the plasma frequency, Gurnett et al. [1979] compared spectral density measurments from a 215 meter dipole antenna on ISEE-1 to measurements from a 30 meter dipole antenna on ISEE-2. It was found that spectral density measurements at the plasma frequency from the two antenna agreed within 10%. Gurnett et al. concluded that plasma oscillations at the plasma frequency have wavelengths longer than the antenna on ISEE-1. A typical electron Debye length in the foreshock region is 9 meters, so plasma oscillations at the plasma frequency satisfy the relation, $k\lambda_{De} << 1$. The long wavelengths of plasma oscillations observed at the plasma frequency were also verified by Anderson et al. [1981] using the same method.

In this study, electric field spectrums obtained from ISEE-1 plasma wave data are compared to ISEE-2 for times when plasma oscillations are observed to shift well below the plasma frequency. Spectrums from over 15 hours of data containing downshift events were compared. An example of this comparison is illustrated in Figure 4. The electric field spectrums were averaged over 20 minutes to obtain the graph illustrated in Figure 4. During the 20-minute interval the spacecraft were 17 km apart and both spacecraft were moving at about 1 km/sec. The long averaging time and the close proximity of ISEE-1 to ISEE-2 were chosen to reduce temporal and spatial aliasing of the separate measurements of the spectral density. For frequencies between 10 kHz and 20 kHz, the spectral densities measured by ISEE-2 are greater than those measured by ISEE-1 by about a factor of 5. At the local plasma frequency (30 kHz), the spectral density measurements from the two spacecraft differ by less than 10%. The difference in the measured spectral densities for frequencies between 10 kHz and 20 kHz is interpreted as an indication that the wavelengths of plasma oscillations below the plasma frequency are between 30 and 215 meters. Since a typical Debye length for the foreshock region is about 9 meters, wavelengths between 30 and 215 meters satisfy $k\lambda_{De} \approx 1$. As a result of study of numerous spectral density comparisons similar to the one illustrated in Figure 4, it is concluded that when the frequency is shifted well below the plasma frequency, plasma oscillations have short wavelengths, $\lambda \approx 2\pi\lambda_{De}$, and when the frequency is at the plasma frequency, plasma oscillations have long wavelengths, $\lambda >> \lambda_{De}$. The

wavelength is assumed to decrease in a continuous manner because plasma oscillations shift in a continuous manner from the plasma frequency to well below the plasma frequency.

Although plasma oscillations below the plasma frequency have short wavelengths, the observed shifts from the plasma frequency can not be attributed entirely to Doppler-shifts. Consider for example, the event illustrated in Figure 3. On October 31, 1977, at 0633 UT, the solar wind velocity was 335 km/second, the number density was 5 cm^{-3} and the electron temperature was 1.1×10^5K. Assuming plasma oscillations with a minimum wavelength of $2\pi\lambda_{De}$, the maximum Doppler shift is estimated to be 5 kHz. The maximum Doppler shift is only about 50% of the observed shift from the plasma frequency in Figure 3. For example, at 0638:50, plasma oscillations are observed at .33 f_{pe}, but plasma oscillations Doppler-shifted from the plasma frequency would occur at or above .7 f_{pe}.

A study was performed to determine where in the foreshock region large deviations from the plasma frequency occur. The three dimensional model of the bow shock used in the study is discussed by Filbert and Kellogg [1979]. The equation for the bow shock is,

$$X = 14.6 - 0.0223\ (Y^2 + Z^2) \qquad (1)$$

where X, Y, and Z are the geocentric solar ecliptic (GSE) coordinates of the bow shock in units of Earth radii. ISEE-1 data pool values for spacecraft coordinates and magnetic field components were used. The

solar wind flow velocity was assumed to be in the $-X_{GSE}$ direction. If the magnetic field was found to intersect the bow shock, then the distance along the solar wind velocity from the tangent field line to the spacecraft field line was computed. This distance is an indication of the depth of penetration of the spacecraft into the foreshock region. A detailed description of the procedure used to determine the spacecraft location in the foreshock region is presented in Appendix A. In this study, 25 hours of wideband data containing over 150 foreshock boundary crossings were used. These events covered a wide range of magnetic field geometries and spacecraft locations.

The characteristics of plasma oscillations were found to depend on the depth of penetration of the spacecraft into the foreshock region. Plasma oscillations are observed at or near the plasma frequency coincident with times when ISEE-1 was within one Earth radii of the foreshock boundary. The observations of plasma oscillations much below the plasma frequency were found to be coincident with times when ISEE-1 was many Earth radii downstream of the foreshock boundary. An example of the correlations discussed above is illustrated in Figure 5. The upper panels of Figure 5 are ISEE-1 wideband data for September 3, 1978 (day 246), 1258 to 1301 UT and 1322 to 1325 UT. The lower panels of Figure 5 are planes defined by the magnetic field averaged over 64 seconds and the solar wind velocity. All downstream convection of electrons to the spacecraft occurs in these planes. As illustrated in Figure 5, ISEE-1 was located about 15 Earth radii downstream of the foreshock boundary at 1300 UT. At this time, the plasma oscillations vary from the plasma

frequency to as much as 10 kHz below the plasma frequency. At 1323 UT, ISEE-1 was less than 1 Earth radii downstream of the foreshock boundary. At this time, the plasma oscillations consist of a narrowband emission at the plasma frequency.

In addition to a study of the correlation between plasma wave data and spacecraft location in the foreshock region, a study of the correlation between plasma wave observations and electron data from the Goddard Space Flight Center electron spectrometer was made. The wave and particle data from over 50 foreshock boundary crossings were compared. The electron spectrometer was chosen for this study because this instrument can detect the electrons responsible for generation of plasma oscillations and reduced one-dimensional distributions can be generated from the electron data.

A good correlation was observed between the shift of plasma oscillations from the plasma frequency and the increase in the flux of energetic electrons at successively lower velocities. One example of this correlation is illustrated in Figure 6. The upper panel of Figure 6 is a plot of iso-contours of constant $F(v_{\parallel})$ for the reduced one dimensional distribution function for electrons propagating upstream from the bow shock. The electron thermal velocity is about 1500 km/sec. A shift of a contour from low to high velocities is an indication of an increase in the flux of electrons. For example, from 1237 - 1238, the contour at 10,000 km/sec shifts to about 12,000 km/sec, indicating an increase in the flux of electrons with velocities equal to 10,000 km/sec. The middle panel is a frequency-time spectrogram. In the

middle panel, the narrowband emissions at 18 kHz are electron plasma oscillations. The lower panel is a plot of the value of Diff, where Diff is defined as the distance from the tangent field line to the spacecraft, measured along the solar wind direction. A large, negative value of Diff implies that the spacecraft is far downstream of the foreshock boundary. A positive value of Diff implies that the spacecraft is on a field line which is not connected to the bow shock.

From 1237:15 to 1239, Diff changes from about -5 R_E to -60 R_E, indicating that the location of ISEE-1 in the foreshock region changes from near the foreshock boundary to far downstream of the foreshock boundary. Coincident with the change of location in the foreshock region, plasma oscillations shift upward to about 1.1 f_{pe}, and then downward to about .7 f_{pe}. As the plasma oscillations shift downward in frequency, the flux of energetic electrons arriving from the bow shock increases at successively lower velocities from 1237:15 to 1239. This trend is illustrated by the first dashed line in the upper panel of Figure 6. From 1240:30 to 1242, Diff changes from about -120 R_E to -5 R_E, indicating that the location of ISEE-1 in the foreshock region changes from far downstream of the foreshock boundary to near the foreshock boundary. The change in the location is accompanied by a shift of plasma oscillations from about .6 f_{pe} to 1.0 f_{pe}. The change in the location is also accompanied by a decrease in the flux of successively higher velocity electrons, as illustrated by the second dashed line in the upper panel of Figure 6. From 1242 to 1244, ISEE-1 is on a magnetic field line which may not be connected to the bow shock. There is

no evidence of electrons from the bow shock with velocities less than 30,000 km/sec in the electron data. The emissions observed at the plasma frequency from 1242 to 1244 may be generated by electrons from the bow shock with velocities greater than 30,000 km/sec or may be enhanced thermal emissions. The intensity of these emissions is four orders of magnitude lower than plasma oscillations that are associated with electrons from the bow shock at 1241. There is no change in the apparent intensity of the emissions in the frequency-time spectrogram because of an automatic gain control on the wideband receiver.

The dark band of noise below 10 kHz in Figure 5 is an artifact of the processing of the wideband data and is not ion acoustic waves. The lack of presence of ion acoustic waves from 1237 to 1245 UT is an indication that there are no ions streaming from the bow shock present for the entire time interval. Since the downshifts of plasma oscillations occur during the time interval, it is concluded that the downshifts are not generated by the presence of ion beams.

The correlation between the increase in the flux of energetic electrons at successively lower velocities and the deeper penetration of the spacecraft into the foreshock region may be an indication that the time-of-flight mechanism discussed by Filbert and Kellogg has an effect on the electron distribution from velocities much greater than the electron thermal velocity to velocities on the order of the electron thermal velocity. This effect is illustrated in Figure 7. When ISEE-1 is far downstream of the foreshock boundary (Figure 7, case 1), the critical velocity may be on the order of the electron thermal

velocity. When ISEE-1 is near the the foreshock boundary (Figure 7, case 2), the critical velocity is much greater than the electron thermal velocity.

An study of electron data for several foreshock boundary crossings was made to determine if unstable distributions of the type reported by Fitzenreiter et al. [1984] are observed when ISEE-1 is in the foreshock region. Reduced one-dimensional distributions that may be unstable to generation of plasma oscillations were found for times when ISEE-1 was located near the foreshock boundary. As the spacecraft penetrated deeper into the foreshock region, the reduced distribution was observed to evolve from a double-peaked distribution to a single-peaked distribution. An example of the time evolution of a reduced distribution is illustrated in Figure 8. The upper part of Figure 8, shows three reduced distributions generated from data taken over 3-second intervals spaced 18 seconds apart. In the lower part of Figure 8, a frequency-time spectrogram and a plot of Diff are illustrated. From 1237:16 to 1238:20, Diff changed from -5.6 R_E to -19.0 R_E, indicating that ISEE-1 was near the electron foreshock boundary. Coincident with this time period at 1237:51, a second peak with a number density of about 10^{-3} - 10^{-4} n_o and a parallel velocity of about 9,500 km/sec is observed in the reduced distribution. In the second distribution, at 1238:09, a plateau at a parallel velocity of about 6,000 km/sec is observed in the reduced distribution. At 1238:27.6, when ISEE-1 is about 25 R_E downstream of the foreshock boundary and plasma oscillations occur below

the plasma frequency, there is no second peak or plateau visible in the reduced distribution.

A simulation of another event similar to the one discussed above was made to determine if the electron spectrometer could detect a low density beam at velocities on the order of the electron thermal velocity. In the simulation, the instrument's velocity space sampling was used to sample a model plasma and beam distribution. It was found that a beam with $n_b = 10^{-2} - 10^{-3}\ n_o$ could be detected for any beam velocity, provided that the beam remained at a fixed velocity for the 3 seconds used to generate a reduced distribution. Reduced distributions can be generated from less than 3 seconds of data, however, coverage of velocity space is reduced and the chances of detecting beams are diminished.

From the study of wideband data similar to that shown in Figure 8, there are indications that plasma oscillations below the plasma frequency may be generated by a beam whose velocity varies significantly over a 3-second time period. Inspection of wideband spectrograms reveals that plasma oscillations below the plasma frequency are time varying emissions spread over a broad range of frequencies. Typically, bursts of less than 50 milliseconds separated by a few tens of milliseconds, are observed. The bandwidths of these bursts are usually about 5 kHz. When these bursts are illustrated in a compressed time format as in Figure 6, they appear continuous. When the time scale is expanded as in Figure 8 at 1238:20 - 1238:35, plasma oscillations below the plasma frequency are bursts of short duration which vary in

frequency. It will be shown in the next sections that, in the context of linear plasma theory, the temporal and frequency variations of plasma oscillations below the plasma frequency are consistent with the interpretation that plasma oscillations are generated by a beam that varies significantly in velocity space on time scales of a few tens of milliseconds. These time scales are much too short for detection of a beam with any electron detector.

Before considering a mechanism for generation of plasma oscillations at, somewhat above, and much below the plasma frequency, a summary of the basic characteristics of the upstream plasma oscillations is given below.

1. Plasma oscillations are observed at frequencies ranging from less than 0.1 f_{pe} to about 1.1 f_{pe}.
2. As plasma oscillations shift below the plasma frequency, their bandwidth increases from a few hundred hertz near the plasma frequency to ±2 kHz well below the plasma frequency.
3. Plasma oscillations at the plasma frequency have wavelengths much greater than a Debye length. Plasma oscillations at frequencies well below the plasma frequency have wavelengths on the order of a few Debye lengths.
4. Plasma oscillations much below the plasma frequency are correlated with times when ISEE-1 is located deep in the foreshock region, far downstream of the foreshock boundary.

5. As plasma oscillations shift from the plasma frequency, the flux of energetic electrons from the bow shock increases at successively lower velocities.
6. The reduced distribution appears to evolve from a double-peaked distribution at the foreshock boundary to a single-peaked distribution downstream of the foreshock boundary. Coincident with this evolution of the reduced distribution plasma oscillations change from continuous and nearly monochromatic emissions at the plasma frequency to time and frequency varying emissions below the plasma frequency.

III. BEAM-PLASMA THEORY

As discussed in the introduction, a mechanism for producing unstable electron distribution functions was demonstrated by Filbert and Kellogg [1979]. They considered an electron distribution at times when a spacecraft is located near the foreshock boundary. For these times, the critical velocity of the beam is much greater than the electron thermal velocity. Downstream of the foreshock boundary, the critical velocity of the beam approaches the electron thermal velocity. To obtain solutions of the linear dispersion relation valid for the entire foreshock region, one must consider a beam-plasma interaction without the restriction that the beam velocity be much greater than the electron thermal velocity. Briggs [1964], Reinleitner et al. [1983], and Grabbe [1984], have considered approximations to the linear dispersion relation and have obtained analytical solutions for $\omega(k)$. In this paper, a numerical solution to the dispersion relation for a plasma and an electron beam will be presented. Solutions to the dispersion relation are obtained for all beam velocities.

Solution of the linear Vlasov equation yields a dispersion relation of the form,

$$D(k,\omega) = 0 = 1 - \sum_s \frac{\omega_{ps}^2}{k^2} \int \frac{\partial F_{os}(v_z)/\partial v_z}{v_z - \frac{\omega}{k}} dv_z \qquad (2)$$

where ω_{ps} is the plasma frequency of the s^{th} species, k is the wave number, $F_{os}(v_z)$ is the reduced one dimensional distribution function for the s^{th} species, and ω is the complex frequency.

The electron distribution in the foreshock region is approximated by a Maxwellian distribution,

$$F_{oe}(v_z) = \left[\frac{1}{2\pi V_t^2}\right]^{1/2} e^{-[v_z^2/2V_t^2]} \tag{3}$$

where V_t is the electron thermal velocity. The electron distribution in the foreshock is more closely approximated by a bi-Maxwellian [Feldman et al., 1975]. However, the results presented below using a single Maxwellian do not differ greatly from the results obtained using a bi-Maxwellian. The electron beam is approximated by a Lorentzian distribution,

$$F_{ob}(v_z) = \frac{C_b}{\pi} \frac{1}{C_b^2 + (v_z - V_b)^2} \tag{4}$$

where C_b is the thermal velocity of the beam and V_b is the beam velocity. Ions are neglected because the downshift of plasma oscillations occur when there are no ions observed streaming from the bow shock and because the solar wind ion distribution has a negligible effect on solutions of the dispersion relation.

Substituting Equation 3 and Equation 4 into Equation 2 and integrating one finds,

$$D(k,\omega) = 0 = 1 + (k\lambda_{De})^2 + zZ(z) - \frac{n_b/n_o(k\lambda_{De})^2}{(k\lambda_{De}V_b/V_t - ik\lambda_{De}T_b/T_e - \omega/\omega_{pe})^2} \cdot \tag{5}$$

Where n_b and n_o are the number density of the beam and the plasma, respectively, T_b and T_e are the temperatures of the beam and the plasma, respectively, $z = \omega/k\ V_t\sqrt{2}$, and $Z(z)$ is the plasma dispersion function [Fried and Conte, 1961].

Equation 5 was solved for $\omega(k)$ numerically using the Muller method [Muller, 1956]. An example of solutions of Equation 5 is illustrated in Figure 9. This illustration shows a graph of, ω_i/ω_{pe} versus ω_r/ω_{pe} for $T_b/T_e = 0$, $n_b/n_o = 0.01$, and $V_b/V_t = 0.5$, 1.0, 2.0, 2.5, and 3.0, where ω_i is the growth rate and ω_r is the frequency. For specific values of V_b/V_t, T_b/T_e, and n_b/n_o, the frequency with the largest growth rate will be the observed frequency. Figure 10 shows the frequency of maximum growth versus V_b/V_t, for $n_b/n_o = 0.01$ and $T_b/T_e = 0$, 0.005, 0.01, 0.05, and 0.1. The wave number of maximum growth versus V_b/V_t for the same values of n_b/n_o and T_b/T_e is illustrated in Figure 11.

The values of n_b/n_o and T_b/T_e were chosen to approximate conditions in the foreshock region. Typically, density ratios are on the order of $10^{-2} - 10^{-3}$. The small temperature ratios were chosen to

approximate the steep positive slope of the electron beams. The steep positive slope is due to the time-of-flight mechanism. From Figure 10 one can see that if the beam temperature changes from $T_b/T_e = 0$ to $T_b/T_e = 0.1$, a downshift of plasma oscillations occurs if $0 < V_b/V_t < 3$. A change in the beam temperature may also occur simultaneously with a change in the beam velocity as the spacecraft penetrates deeper into the foreshock region. An indication of a change in the beam temperature is illustrated in Figure 6. From 1238:30 to 1239, the contours of the reduced distribution at velocities less than 5000 km/sec shift more gradually as ISEE-1 penetrates more deeply into the foreshock region. The more gradual shift in the contours may be an indication that the steep positive slope of the time-of-flight distribution occurs near the foreshock boundary and becomes less steep as ISEE-1 moves into the foreshock region. Such a change in the steepness may increase downshifts of plasma oscillations from the plasma frequency.

Analytical solutions to the dispersion relation can be obtained by considering two limiting forms of Equation 5. By obtaining these solutions, the influence of various parts of the dispersion relation on the frequency of maximum growth is illustrated. The limiting forms of Equation 5, for slightly different initial conditions, are discussed by Briggs [1964] and Grabbe [1984].

The first limiting form of Equation 5 can be obtained by assuming $V_b/V_t \gg 1$. This limiting form is equivalent to the high phase velocity approximation, $\omega/k \gg V_t$. Using the high phase velocity approximation for the plasma dispersion function (and in the limit of $\omega_i \to 0$), Equation 5 can be approximated as,

$$D(k,\omega) = 0 \approx 1 - \frac{\omega_{pe}^2}{\omega^2} - \frac{3\,\omega_{pe}^4 (k\lambda_{De})^2}{\omega^4} - \frac{n_b/n_o (k\lambda_{De})^2}{(k\lambda_{De} V_b/V_t - \omega/\omega_{pe})^2} \qquad (6)$$

where the additional assumption of a cold beam $T_b/T_e \to 0$ has been made. The third term in Equation 6 is a result of choosing a Maxwellian distribution for the electrons. By neglecting the third term, Equation 6 can be solved for small n_b/n_o using the weak beam approximation [Mikhailovskii, 1974]. Assuming $\omega_r = \omega_{pe} + \delta\omega$, one finds,

$$\omega_r \approx \omega_{pe}\left(1 - \frac{1}{2\sqrt[3]{2}}\, n_b/n_o^{2/3}\right) \qquad (7)$$

Neglecting the fourth term in Equation 6 instead of the third term, one finds the solution to the resulting Equation is [Bohm and Gould, 1949],

$$\omega_r^2 \approx \omega_{pe}^2(1 + 3(k\lambda_{De})^2) \qquad (8)$$

The curve illustrated in Figure 9 for values of $V_b/V_t > 3$ results from a combination effects illustrated by Equations 7 and 8. For $2 < V_b/V_t < 4$, $k\lambda_{De}$ is slightly less than one, so the approximation used to obtain Equation 8 is valid resulting in $\omega_r > \omega_{pe}$. For $V_b/V_t > 4$, $k\lambda_{De}$ is much less than one, so the approximation used to obtain Equation 7 is valid resulting in $\omega_r < \omega_{pe}$. If the beam density becomes a significant fraction of the plasma density, one can see that $\omega_r << \omega_{pe}$ could

result. This case is not considered because the typical beam densities in the foreshock region are very small compared to the plasma densities.

The second limiting form of Equation 5 is obtained by assuming $V_b/V_t \ll 1$. This limit is equivelent to the low phase velocity limit, $\omega_r/k \ll V_t$. For $\omega_r/k \ll V_t$ and $\omega_i \to 0$, $zZ(z) \approx 0$, so Equation 5 is approximated by,

$$D(k,\omega) = 0 \approx 1 + (k\lambda_{De})^2 - \frac{n_b/n_o (k\lambda_{De})^2}{(k\lambda_{De} V_b/V_t - \omega/\omega_{pe})^2} \qquad (9)$$

where the additional assumption of a cold beam, $T_b/T_e \to 0$, has been made. Solving this equation for ω_r one finds,

$$\omega_r \approx \omega_{pe}\, k\lambda_{De} \left(V_b/V_t \pm \left(\frac{n_b/n_o}{1 + (k\lambda_{De})^2}\right)^{1/2}\right) \qquad (10)$$

The general shape of the curve in Figure 9 can be predicted using the approximations to the frequency of maximum growth in Equations 7, 8, and 10. From Equation 10 one can see that if $V_b/V_t \ll 1$ and $n_b/n_o \ll 1$, then $\omega_r/\omega_{pe} \ll 1$ and from Equation 8 one can see that if $V_b/V_t \approx 3$, then $\omega_r/\omega_{pe} > 1$. Thus, the curve of ω_r/ω_{pe} versus V_b/V_t is predicted to vary smoothly from $\omega_r/\omega_{pe} \approx 0$ and $V_b/V_t \approx 0$ to $\omega_r/\omega_{pe} > 1$ and $V_b/V_t \approx 3$. From Equation 7, one can see that if $V_b/V_t \gg 1$, then

$\omega_r/\omega_{pe} < 1$. Thus the curve of ω_r/ω_{pe} versus V_b/V_t is predicted to vary smoothly from $\omega_r/\omega_{pe} > 1$ and $V_b/V_t \approx 3$ to $\omega_r/\omega_{pe} < 1$ and $V_b/V_t >> 1$.

The solutions in Equations 7, 8, and 10 are only approximate and breakdown when $V_b/V_t \approx 1$, so one must solve the full dispersion relation (Equation 5) numerically as was done to obtain Figures 9, 10 and 11.

IV. COMPARISON OF THEORY TO OBSERVATIONS

In this section, the observations of plasma oscillations summarized at the end of Section II are compared to the predictions from the beam-plasma theory presented in Section III.

Plasma oscillations are observed at frequencies ranging from less than 0.1 f_{pe} to about 1.1 f_{pe}. In Figure 10, the observed frequency range is reproduced by an electron beam that varies in velocity from $V_b/V_t \gg 1$ to $V_b/V_t \approx 1$. The time-of-flight mechanism causes the beam velocity variation. When the spacecraft is near the foreshock boundary, only high velocity electrons reach the spacecraft, resulting in $V_b/V_t \gg 1$. Far downstream of the foreshock boundary, electrons with velocities on the order of the electron thermal velocity reach the spacecraft, resulting in $V_b/V_t \approx 1$. Thus, the beam-plasma interaction and the time-of-flight mechanism combine to produce plasma oscillations in the observed frequency range.

As plasma oscillations shift below the plasma frequency, their bandwidth increases from a few hundred hertz near the plasma frequency to ±2 kHz well below the plasma frequency. This increase in bandwidth may be produced by a small fluctuation in the beam velocity. A small fluctuation in the beam velocity could occur in the foreshock region because of changes in the magnetic field geometry. The effect of a small fluctuation in the beam velocity is understood by considering

Figure 10. For $V_b/V_t > 4$, the curve of ω_r/ω_{pe} versus V_b/V_t has near zero slope. For a small fluctuation in the beam velocity, plasma oscillations are generated over a narrow range of frequencies centered near the plasma frequency. For $V_b/V_t \approx 1$, the curve of ω_r/ω_{pe} versus V_b/V_t has a large, positive slope. For a small fluctuation in the beam velocity, plasma oscillations are generated over a broad range of frequencies centered well below the plasma frequency.

The increase in the bandwidth as plasma oscillations shift below the plasma frequency may also be a consequence of the nature of the solutions of the dispersion relation. From Figure 8, it is concluded that when $V_b/V_t = 3$, plasma oscillations are narrow band emissions near the plasma frequency because the growth rate versus frequency is sharply peaked near the plasma frequency. When $V_b/V_t = 1$, plasma oscillations may occur over a broad range of frequencies because the growth rate varies by a small amount over a broad range of frequencies centered well below the plasma frequency. Thus, the change in bandwidth may be either a consequence of the nature of the solutions to the dispersion relation or may be a result of a fluctuation in the beam velocity.

Plasma oscillations at the plasma frequency have wavelengths much greater than a debye length. Plasma oscillations at frequencies well below the plasma frequency have wavelengths on the order of a few debye lengths. The change in wavelength as plasma oscillations shift below the plasma frequency is illustrated in Figures 10 and 11. For $V_b/V_t \gg 1$, plasma oscillations occur near the plasma frequency and have long wavelengths, $(k\lambda_{De} \ll 1)$. As V_b/V_t decreases plasma

oscillations shift first above, then below the plasma frequency and the wavelengths shift from $\lambda >> \lambda_{De}$ to $\lambda \approx \lambda_{De}$. One can understand why the wavelengths of plasma oscillations well below the plasma frequency are greater than the 30 meter electric antenna on ISEE-2 and less than the 215 meter electric antenna on ISEE-1 by considering some typical plasma parameters for the foureshock region. If one considers a typical electron temperature and number density of 1.5×10^5K and 9 cm^{-3}, respectively, then λ_{De} = 9 meters. If $2\pi\lambda_{De}$ is used as the criteria for the minimum wavelength in the plasma, then λ_{min} = 56 meters. This minimum wavelength is greater than the length of the 30 meter electric antenna on ISEE-2 but less than the length of the 215 meter antenna on ISEE-1. For λ = 215 meters, $k\lambda_{De}$ = 0.23. Referring to Figure 11, if $k\lambda_{De}$ = 0.23, then for $V_b/V_t < 4$, the wavelengths of plasma oscillations are less than 215 meters. When the spacecraft is located deep in the foreshock region, as in the example illustrated in Figure 4, $V_b/V_t < 4$ is satisfied, so the wavelengths are between 30 and 215 meters. One can see that the observed wavelengths of plasma oscillations at and below the plasma frequency are predicted using the beam-plasma theory.

Plasma oscillations much below the plasma frequency are correlated with times when ISEE-1 is located deep in the foreshock region, far downstream of the foreshock boundary. This correlation can be understood by considering in Figure 7. When ISEE-1 is located near the foreshock boundary (case 1), V_b/V_t is much greater than one, resulting in plasma oscillations at the plasma frequency. When ISEE-1 is located

deep in the foreshock region (case 2), V_b/V_t is approximately equal to one, resulting in plasma oscillations well below the plasma frequency.

The critical velocity can be computed using the equation, [Filbert and Kellogg, 1979]

$$V_c = \frac{D \cdot V_{sw}}{Diff} \tag{11}$$

where V_c is the critical velocity, D is the distance from the tangent point to the spacecraft, Diff is the distance from the spacecraft to the tangent field line along the solar wind velocity direction, and V_{sw} is the solar wind velocity. For the event in Figure 5, at 1300 UT, $V_c \approx 0.9\ V_t$. Since $V_b/V_t < 1$, plasma oscillations are expected and observed below the plasma frequency. In Figure 5, for the event at 1323 UT, $V_c \approx 6\ V_t$. Since $V_c \approx 6\ V_t$, plasma oscillations are expected and observed at the plasma frequency. Thus, a comparison of the observed frequencies of plasma oscillations is in agreement with the predicted critical velocities.

As plasma oscillations shift from the plasma frequency, the flux of energetic electrons from the bow shock shifts from velocities much greater than the electron thermal velocity to velocities on the order of the electron thermal velocity. This shift in velocity is interpreted as an indication that the time-of-flight mechanism discussed by Filbert and Kellogg is valid not only near the foreshock boundary, but is also valid far downstream of the foreshock boundary. Thus,

plasma oscillations throughout the foreshock region are generated by a beam-plasma interaction.

The reduced distribution appears to evolve from a double-peaked distribution at the foreshock boundary to a single-peaked distribution downstream of the foreshock boundary. Coincident with the evolution of the reduced distribution, plasma oscillations change from continuous and nearly monochromatic emissions at the plasma frequency, to time and frequency varying emissions below the plasma frequency. This apparent evolution from a double-peaked distribution to a single-peaked distribution is the only observation in this thesis that is inconsistent with the beam-plasma theory presented in Section 3. In the context of linear plasma theory, the single-peaked distribution observed downstream of the foreshock boundary does not have a free energy source capable of driving electron plasma oscillations. The fact that plasma oscillations are observed downstream of the foreshock boundary may be an indication that a beam is present in the reduced distribution. Using a model distribution for the event illustrated in Figure 8, it was found that the Goddard Space Flight Center Electron Spectrometer was capable of detecting a beam with any velocity, provided that the beam remained at a fixed velocity for three seconds used to generate a reduced distribution. The observations of short duration bursts of plasma oscillations such as those illustrated in Figure 8 at 1238:20 - 1238:35 are an indication that downstream of the foreshock boundary, the generation of plasma oscillations occurs on much shorter time scales than 3 seconds. A typical burst lasts less than 50 milliseconds and has a

bandwidth of 5 kHz. As pointed out above, a fluctuation in the beam velocity could account for the 5 kHz bandwidth of the bursts. Any 3 second time period may contain 20-40 bursts at varying frequencies. In the context of the beam-plasma theory in Section III, bursts of plasma oscillations at different frequencies are generated by bursts of electrons at different velocities. When averaged over 3 seconds, the bursts of electrons at different velocities would appear only as an enhancement in the flux of upstreaming electrons.

Examples of model reduced distributions obtained by averaging beams at different velocities are illustrated in Figure 12. The solid line in all three panels is a representation of the solar wind distribution. The solar wind distribution is modeled by two Maxwellians [Feldman et al., 1975]. In the first panel, a Maxwellian beam, with a velocity of -10,000 km/sec and a number density of about 10^{-3} is added to the model solar wind distribution. The resulting model distribution in the first panel is comparable to the observed distribution near the foreshock boundary (distribution A, Figure 8). In the second distribution, an average of 6 beams is added to the model solar wind distribution. These 6 beams have beam velocities ranging from -8,000 km/sec to -3,000 km/sec with beam temperature and beam density increasing as beam velocity decreases. The resulting model distribution has a plateau at a parallel velocity of about -6,000 km/sec. This plateau is similar to the plateau observed in distribution B in Figure 8. In the third panel, an average of 6 beams is added to the model solar wind distribution. These 6 beams have beam velocities varying from -6,000 km/sec to

-10,000 km/sec with beam temperature and beam density increasing as velocity decreases. The resulting model distribution shows only an enhancement of parallel velocities from -12,000 km/sec to -6,000 km/sec. This enhancement is similar to the enhancement observed in distribution C in Figure 8.

Model distributions B and C in Figure 8 serve to illustrate that an average of several beams at different velocities could result in a distribution that does not have a positive slope. The averaging of the electron spectrometer is much more complicated than the simple averaging used to generate the model distributions in Figure 12. The more complicated averaging arises because the time it takes the instrument to make one energy step (~ 20 milliseconds) is comparable with the duration of the electron bursts (~ 50 milliseconds). Thus, the electron instrument samples only a small part of the three dimensional distribution in the time it takes the distribution to change. As a result, the observed reduced distribution is an average of small portions of many different distributions. This averaging will degrade features like a sharp positive slope in the distribution.

Further study of the wave and particle data is needed to confirm evidence that temporal variations of an electron beam are the reason why reduced distributions far downstream of the foreshock boundary do not appear to have clearly defined electron beams. It may be found that other nonlinear instabilities which do not require an electron beam will be consistent with some observed characteristics of plasma oscillations. However, the linear beam-plasma instability presented in

this thesis is the most likely generation mechanism at present because the predictions from this mechanism agree with the observed characteristics of plasma oscillations in the foreshock region.

REFERENCES

Anderson, K. A., Energetic electrons of terrestrial origin upstream in the solar wind, J. Geophys. Res., 73, 2387, 1968.

Anderson, K. A., Energetic electrons of terrestrial origin behind the bow shock and upstream in the solar wind, J. Geophys. Res., 74, 95, 1969.

Anderson, R. R., G. K. Parks, T. E. Eastman, D. A. Gurnett, and L. A. Frank, Plasma waves associated with energetic particles streaming into the solar wind from the Earth's bow shock, J. Geophys. Res., 86, 4493, 1981.

Bohm, D., and E. P. Gross, Theory of plasma oscillations. A. Origin of medium-like behavior, Phys. Rev., 75, 1851, 1949.

Briggs, Richard J., Electron-stream interaction with plasmas, M.I.T. Press, Cambridge, MA, 1964.

Fairfield, D. M., Average and unusual locations of the Earth's magnetopause and bow shock, J. Geophys. Res., 76, 6700, 1971.

Feldman, W. C., J. R. Asbridge, S. J. Bame, M. D. Montgomery, and S. P. Gary, Solar wind electrons, J. Geophys. Res., 80, 4181, 1975.

Filbert, P. C., and P. J. Kellogg, Electrostatic noise at the plasma frequency beyond the Earth's bow shock, J. Geophys. Res., 84, 1369, 1979.

Fitzenreiter, R. J., A. J. Klimas, and J. D. Scudder, Detection of bump-on-tail reduced electron velocity distributions at the electron foreshock boundary, Geophys. Res. Lett., 11, 496, 1984.

Fredricks, R. W., C. F. Kennel, F. L. Scarf, G. M. Crook, and I. M. Green, Detection of electric-field turbulence in the Earth's bow shock, Phys. Rev. Lett., 21, 1761, 1968.

Fredricks, R. W., F. L. Scarf, and L. A. Frank, Nonthermal electrons and high-frequency waves in the upstream solar wind. 2. Analysis and interpretation, J. Geophys. Res., 76, 6691, 1971.

Fredricks, R. W., F. L. Scarf, C. T. Russell, and M. Neugebauer, Detection of solar-wind electron plasma frequency fluctuations in an oblique nonlinear magnetohydrodynamic wave, J. Geophys. Res. Lett., 77, 3598, 1972.

Grabbe, C. L., A model for chorus associated electrostatic bursts, J. Geophys. Res., 89, 919, 1984.

Gurnett, D. A., R. R. Anderson, F. L. Scarf, R. W. Fredricks, E. J. Smith, Initial results from the ISEE-1 and -2 plasma wave investigation, Space Sci. Rev., 23, 103, 1979.

Gurnett, D. A., and L. A. Frank, Electron plasma oscillations associated with Type III radio emissions and solar electrons, Solar Phys., 45, 477, 1975.

Gurnett, D. A., F. L. Scarf, R. W. Fredricks, E. J. Smith, The ISEE-1 and ISEE-2 plasma wave investigation, IEEE Trans. Geosci. Electr., GE-16, 225, 1978.

Mikhailovskii, A. B., Theory of Plasma Instabilities (Vol. 1: Instabilities of a Homogeneous Plasma), Consultants Bureau, New York-London, 1974.

Muller, D. E., A method for solving algebraic equations using an automatic computer, Math. Comp., 10, 208, 1956.

Ogilvie, K. W., J. D. Scudder, and H. Doong, The electron spectrometer experiment on ISEE-1, IEEE Trans. Geosci. Electr., GE-16, 261, 1978.

Reinleitner, L. A., D. A. Gurnett, T. E. Eastman, Electrostatic bursts generated by electrons in Landau resonance with whistler mode chorus, J. Geophys. Res., 88, 3079, 1983.

Rodriguez, P., and D. A. Gurnett, Electrostatic and electromagnetic turbulence associated with the Earth's bow shock, J. Geophys. Res., 80, 19, 1975.

Rodriguez, P., and D. A. Gurnett, Correlation of bow shock plasma wave turbulence with solar wind parameters, J. Geophys. Res., 81, 2871, 1976.

Scarf, F. L., R. W. Fredricks, L. A. Frank, and M. Neugebauer, Nonthermal electrons and high-frequency waves in the upstream solar wind. 1. Observations, J. Geophys. Res., 76, 5162, 1971.

Scarf, F. L., R. W. Fredricks, L. A. Frank, C. T. Russell, P. J. Coleman, Jr., and M. Neugebauer, Direct correlations of large amplitude waves with suprathermal protons in the upstream solar wind, J. Geophys. Res., 75, 7316, 1970.

APPENDIX A

SPACECRAFT POSITION
RELATIVE TO THE TANGENT FIELD LINE

An important part of this thesis was the study of the correlation between the shifts of plasma oscillations from the plasma frequency and the location of ISEE-1 in the foreshock region. To study this correlation, a computer program was written to determine the location of ISEE-1 in the foreshock region given the magnetic field components at the spacecraft, the Geocentric Solar Ecliptic (GSE) coordinates of the spacecraft, and an equation for the bow shock. Filbert and Kellogg [1979] discuss a procedure for determining the location of the spacecraft relative to the bow shock. Some approximations in their procedure were unnecessary. In the procedure outlined below, the approximations used by Filbert and Kellogg are not made.

The bow shock surface is represented by a paraboloid of revolution about the X-axis [Fairfield, 1971],

$$X = X_o + K(Y^2 + Z^2) \quad . \tag{A1}$$

The magnetic field is represented by a vector,

$$\vec{B} = (B_x, B_y, B_z) \quad . \tag{A2}$$

The spacecraft location relative to the magnetic field line that is tangent to the bow shock is obtained by determining the following:

1) If the spacecraft is on a magnetic field line that does not intersect the bow shock, then find the distance of closest approach of the spacecraft field line to the bow shock.
2) If the spacecraft is on a field line that does intersect the bow shock, then find the the distance from the tangent field line to the spacecraft?

The two possibilities are illustrated in two dimensions in Figure 12. If the spacecraft is on a magnetic field line that does not intersect the bow shock, then Diff is the length of the line segment perpendicular to both the bow shock and the magnetic field line. If the spacecraft is on a magnetic field line that does intersect the bow shock, then Diff is the distance from the tangent magnetic field line to the spacecraft, measured along the solar wind direction. In the right panel of Figure 12, the value of Diff is used to determine the value for the critical velocity for electrons streaming from the tangent point.

To simplify the determination of the location of the spacecraft relative to the bow shock, the GSE coordinate system is first rotated about the Earth-Sun line (X_{GSE} axis) so that the magnetic field is parallel to the X-Y plane. Using the rotated coordinate system, the equation for the magnetic field line in parametric form is,

$$X = B_x t + X_s \tag{3A}$$

$$Y = B'_y t + Y'_s \tag{4A}$$

$$Z = Z'_s \quad . \tag{5A}$$

Where X_s, Y'_s, Z'_s are the rotated coordinates of the spacecraft, B_x and B'_y are the rotated magnetic field components, and t is the parameter of the line.

If the magnetic field line intersects the bow shock, then at least one set of values for X, Y, Z and t can be found that satisfies Equation 1A, and Equations 3A-5A. Solving Equations 1A, 3A-5A for t, one finds,

$$t = \frac{B_x - 2KB'_y Y'_s}{2KB'^2_y} \pm \sqrt{\frac{B_x^2 + 4KB'_y(B'_y X_s - B'_y X_o - KB'_y Z'^2_s - Y'_s(B'_x)}{2KB'^2_y}} \tag{6A}$$

Using Equation 6A one can determine whether or not the magnetic field line intersects the bow shock. If the quantity under the square root in Equation 6A is less than zero, then the magnetic field line does not intersect the bow shock. If it is positive, then the magnetic field line intersects the bow shock twice.

In the case of no intersection, the distance of closest approach is determined by finding the gradient of the paraboloid that intersects

the magnetiac field line perpendicularly, as illustrated in the left panel of Figure 12. When the gradient of Equation 1 is taken one finds,

$$\vec{\nabla}F = (1, -2KY, -2KZ) \quad . \tag{7A}$$

The condition that the gradient be perpendicular to the magnetic field line can be expressed as,

$$\vec{\nabla}F \cdot \vec{B}' = 0 \tag{8A}$$

with,

$$\vec{B}' = (B_x, B'_y, 0) \quad . \tag{9A}$$

From Equations 2A, 8A and 9A the value of Y on the parabola is

$$Y_p = \frac{B_x}{2KB'_y} = \frac{1}{2Ka} \tag{10A}$$

where a is the slope of the magnetic field line in the X-Y plane.

To find the other components (X_p, Z_p, X_L, Y_L, Z_L) of the shortest line segment between the paraboloid in Equation 1A and the magnetic

field line, one uses Equations 7A and 10A to write the equation of the line segment that is perpendicular to the paraboloid in parametric form

$$X = X_p + t \tag{11A}$$

$$Y = Y_p - 2KY_p t \tag{12A}$$

$$Z = Z_p - 2KZ_p t \quad . \tag{13A}$$

If the line segment that is perpendicular to both the bow shock and the magnetic field line, intersects the magnetic field line, then

$$X_L = X_p + t \tag{14A}$$

$$Y_L = Y_p - 2KY_p t \tag{15A}$$

$$Z_L = Z_p - 2KZ_p t \tag{16A}$$

must be true. Since the value of Y_p is known from Equation 10A, Equations 14A-16A contains 6 unknowns; X_L, Y_L, Z_L, X_p, Z_p, and t. The other three equations needed to have a set of six equations with six unknowns are the equations for the magnetic field line and the paraboloid,

$$X_L = aY_L + b \tag{17A}$$

$$Z_L = Z_S' \tag{18A}$$

$$X_p = X_o + K(Y_p^2 + Z_p^2) \tag{19A}$$

using Equations 10A and 14A-19A, the values of X_L, Y_L, Z_L, X_p, Y_p, Z_p, and t can be determined, and the length of the line segment is

$$\text{Diff} = \sqrt{(X_L - X_p)^2 + (Y_L - Y_p)^2 + (Z_L - Z_p)^2} \tag{20A}$$

If the magnetic field line intersects the bow shock, then Diff is defined as the length of the line segment along the solar wind direction from the tangent field line to the spacecraft, as illustrated in the right panel of Figure 13. This distance is determined by first computing the values of X_p and Y_p from Equations 10A and 14A-19A. The magnetic field line that is tangent to the bow shock and parallel to the spacecraft magnetic field line has the same slope as the spacecraft magnetic field line but passes through the point (X_p, Yp). This tangent field line can be written as

$$X = aY + b' \quad . \tag{21A}$$

Substituting X_p, Y_p into Equation 21A, one can solve for b'. Once b' is known, the value of Y_b' is substituted into Equation 21A to determine the value of X on the tangent magnetic field line,

$$X_T = aY'_s + b' \quad . \tag{22A}$$

The value of Diff in the case of two intersections is

$$\text{Diff} = |X_S - X_T| \quad . \tag{23A}$$

APPENDIX B

FIGURES

Figure 1 Electrons streaming from the bow shock are convected downstream due to the motion of the solar wind. Electrons originating from the tangent point with very high energies define a boundary called the electron foreshock boundary. Downstream of this boundary is a region called the electron foreshock region. In this region the "beam" of electrons originating from the bow shock has a characteristic lower cutoff velocity. This cutoff velocity occurs because electrons below a certain critical velocity are convected downstream before they reach the spacecraft.

A-G84-80-1

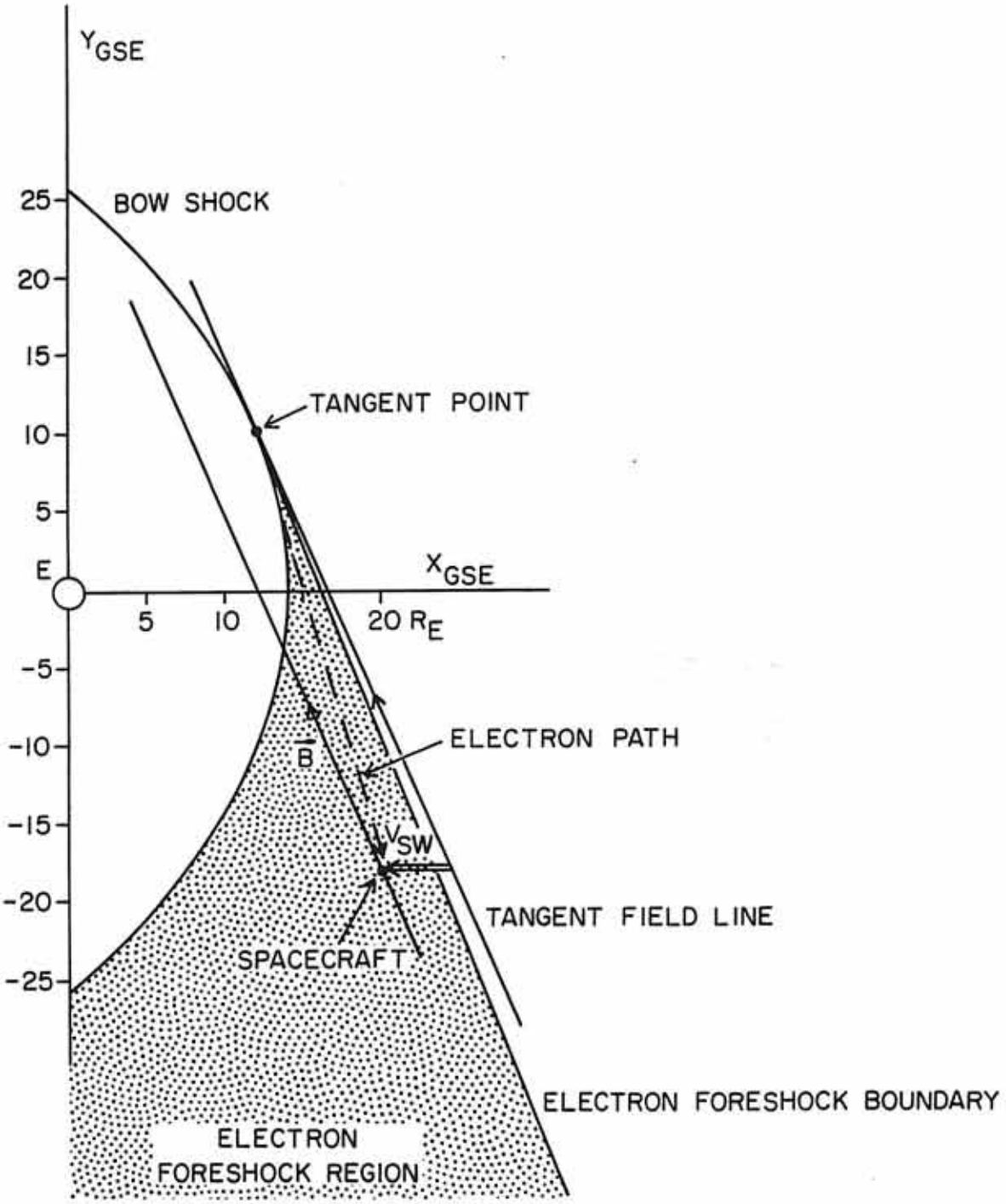

Figure 1

Figure 2 A frequency-time spectrogram from ISEE-1. Fluctuations in the plasma frequency may be caused by the presence of oblique, nonlinear magnetohydrodynamic waves. The presence of ion acoustic waves indicates the presence of ions streaming from the bow shock. These ions are believed to provide the free energy source needed to drive the MHD waves.

A-G84-104-3

ISEE-1 WIDEBAND DATA
AUGUST 15, 1978 DAY 227
R = 22 R_E LOCAL TIME = 15.2 HRS

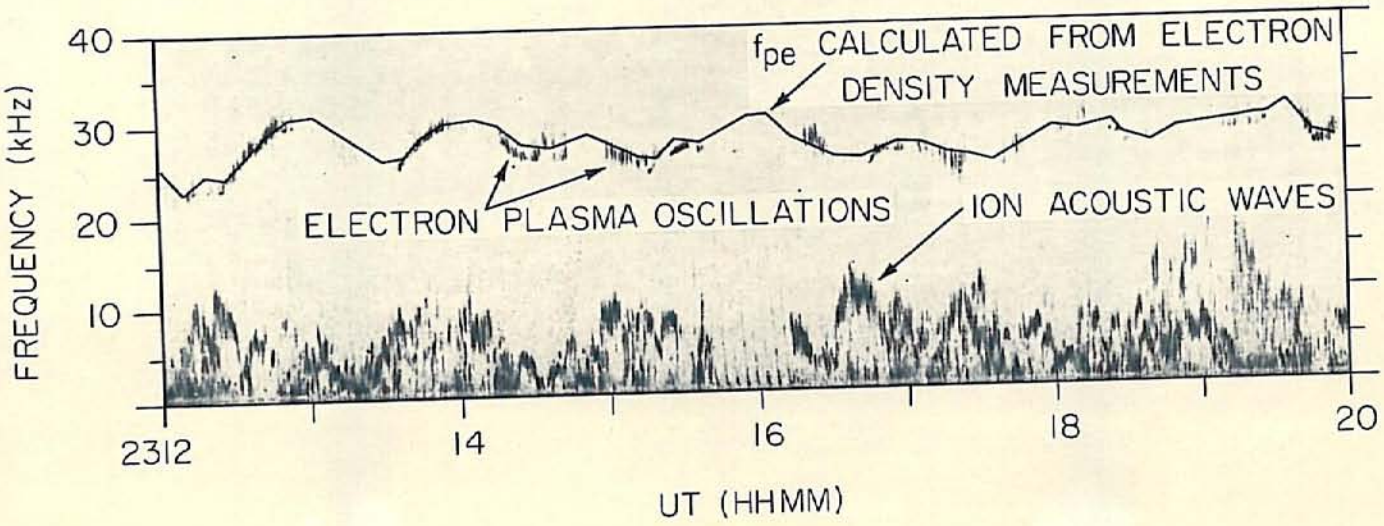

Figure 2

Figure 3 The upper panel is a frequency-time wideband spectrogram from the ISEE-1 wideband receiver taken when the spacecraft was located in the foreshock region. The lower panel is a plot of the plasma frequency determined from electron density measurements. From 0633 to 0633:30 and from 0638:30 to 0639, plasma oscillations are observed to shift well below the plasma frequency. Coincident with these shifts is an increase in the bandwidth of the emissions from a few hundred Hz at the plasma frequency to ±2 kHz well below the plasma frequency.

C-G84-110-3

ISEE-1 WIDEBAND DATA
OCTOBER 31, 1977 DAY 304
R = 22 R_E LOCAL TIME = 11 HRS

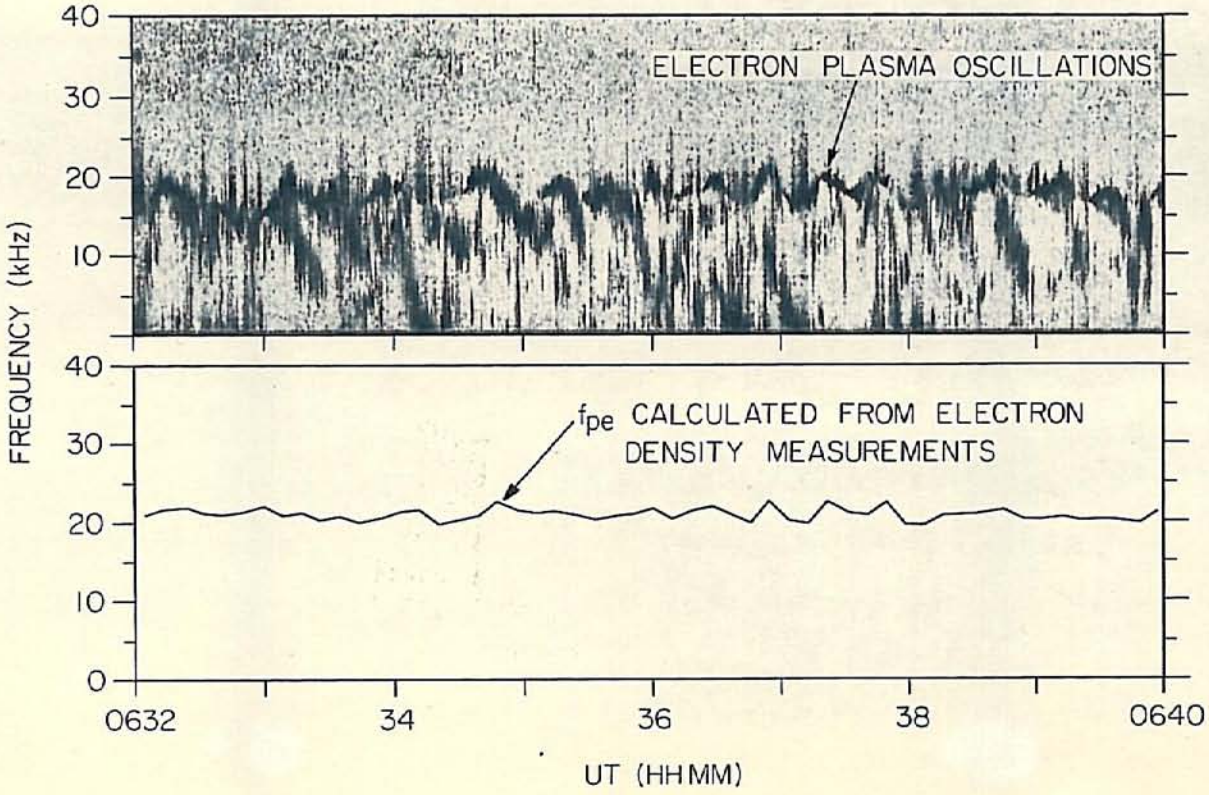

Figure 3

Figure 4 A plot of a 20-minute average spectral density versus frequency, for an event when plasma oscillations occurred well below the plasma frequency. The plasma frequency for this event was about 30 kHz. For frequencies between 10 and 20 kHz, the spectral density from ISEE-2 is greater than that from ISEE-1 by about a factor of 5. This difference indicates that the wavelengths of the plasma oscillations well below the plasma frequency are shorter than the ISEE-1 antenna (215 meters) and longer than the ISEE-2 antenna (30 meters).

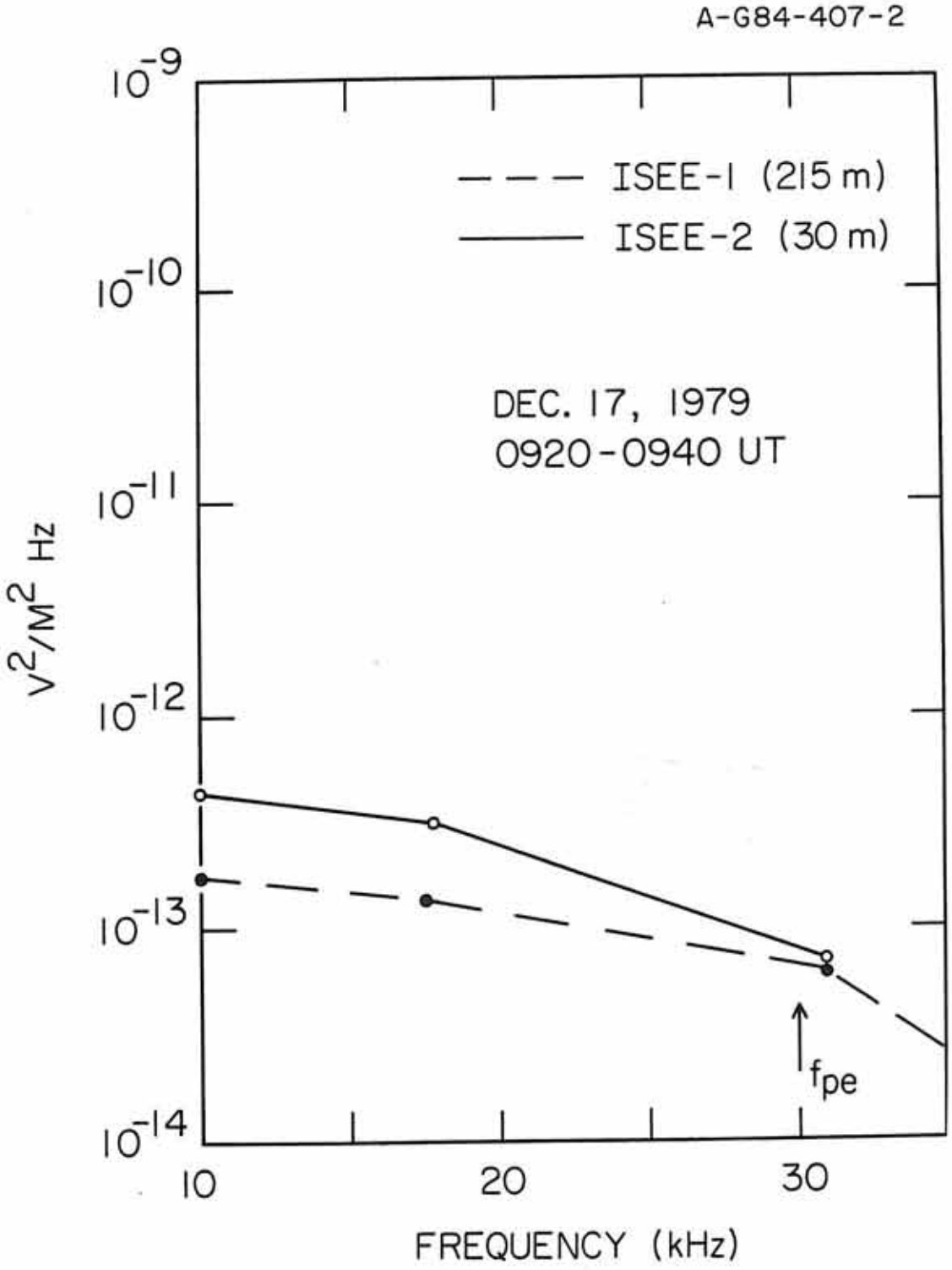
A-G84-407-2
ISEE-1 (215 m)
ISEE-2 (30 m)
DEC. 17, 1979
0920-0940 UT
10^{-9}
10^{-10}
10^{-11}
10^{-12}
10^{-13}
10^{-14}
V^2/M^2 Hz
f_{pe}
10
20
30
FREQUENCY (kHz)

Figure 4

Figure 5 Plasma oscillations are observed below the plasma frequency coincident with times when ISEE-1 is located far downstream of the electron foreshock boundary. In the left panel, from 1259:15 to 1300:19, ISEE-1 was about 15 Earth radii from the foreshock boundary. Coincident with this time, plasma oscillations occur well below the plasma frequency. In the right panel, from 1322:45 to 1323:49, ISEE-1 was located less than one Earth radii from the foreshock boundary. Coincident with this time, plasma oscillations occur at the plasma frequency.

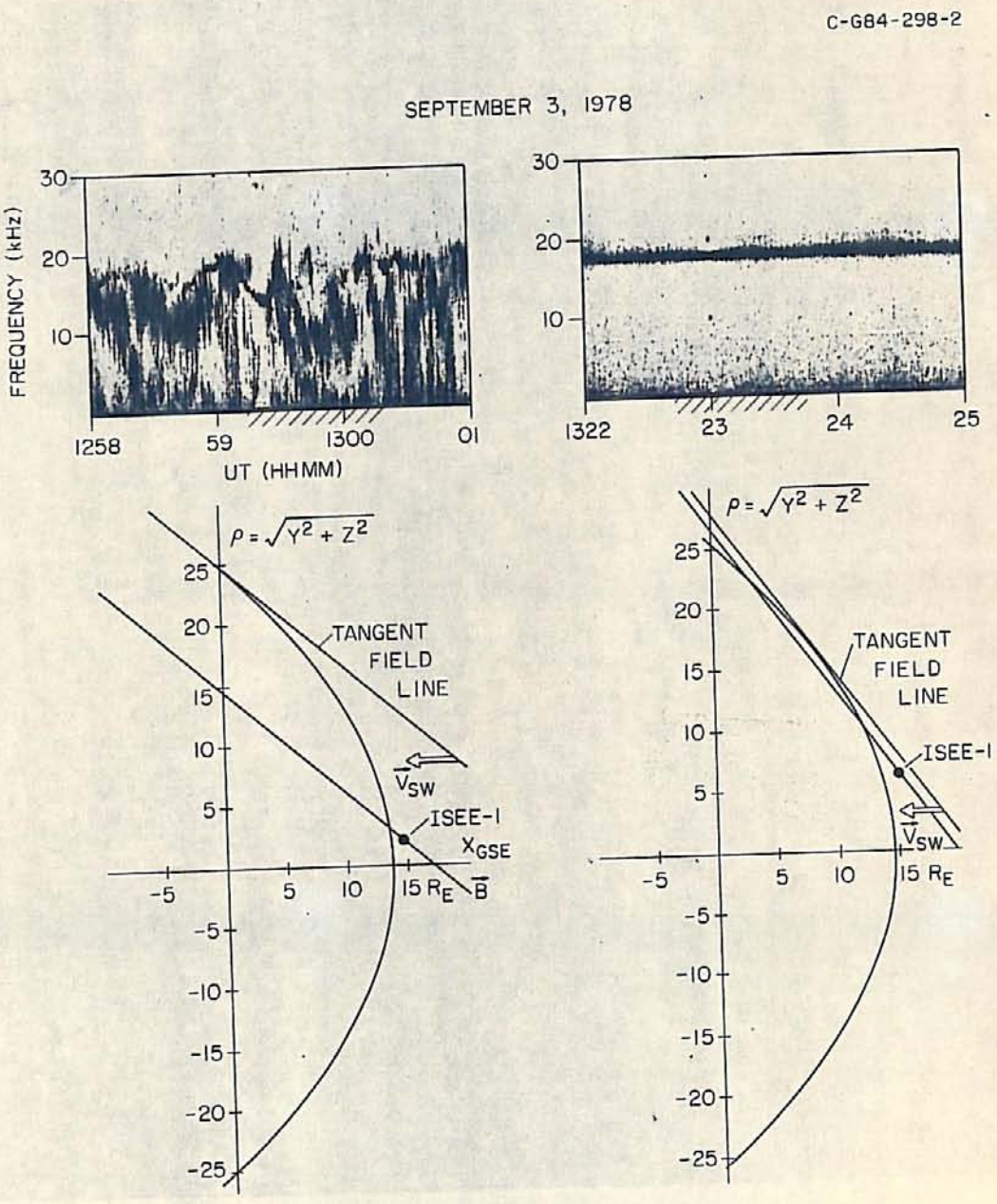
C-G84-298-2
SEPTEMBER 3, 1978
FREQUENCY (kHz)
30
20
10
1258
59
1300
01
UT (HHMM)
1322
23
24
25
$\rho = \sqrt{Y^2 + Z^2}$
TANGENT FIELD LINE
V_{SW}
ISEE-1
X_{GSE}
$\vec{B}$
15 R_E
-5
5
10
15
-10
-15
-20
-25

Figure 5

Figure 6 The upper panel is a plot of iso-contours of the reduced one-dimensional distribution for electrons propagating upstream from the bow shock. A shift of a contour from low to high velocities is an indication of an increase in the flux of electrons at low velocities. The middle panel is a frequency-time spectrogram. The narrowband emissions at 18 kHz are electron plasma oscillations. The lower panel is a plot of Diff. A large, negative value of Diff implies that ISEE-1 is far downstream of the foreshock boundary. From 1237 to 1239, ISEE-1 penetrates deeply into the foreshock region, the flux of energetic electrons shifts to lower velocities, and plasma oscillations shift first above, then below the plasma frequency. The reverse happens from 1240 to 1242.

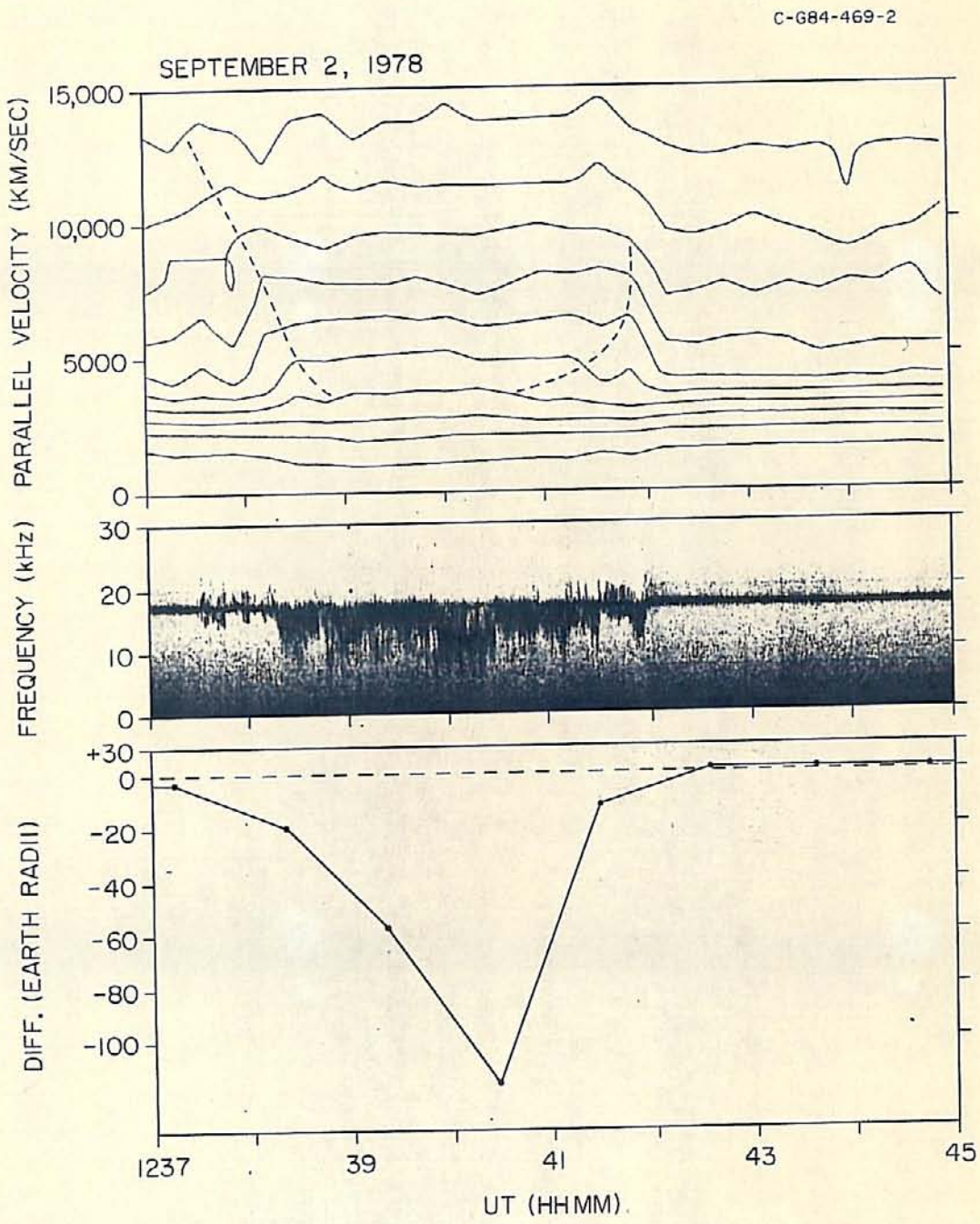
C-G84-469-2
SEPTEMBER 2, 1978
PARALLEL VELOCITY (KM/SEC)
15,000
10,000
5000
0
FREQUENCY (kHz)
30
20
10
0
DIFF. (EARTH RADII)
+30
0
-20
-40
-60
-80
-100
1237
39
41
43
45
UT (HHMM)

Figure 6

Figure 7 The reduced one-dimensional distribution depends on the spacecraft location in the foreshock region. When the spacecraft is located far downstream the foreshock boundary (case 1), the critical velocity is on the order of the electron thermal velocity. When the spacecraft is located near the foreshock boundary, (case 2), the critical velocity is much greater than the electron thermal velocity.

A-G84-408

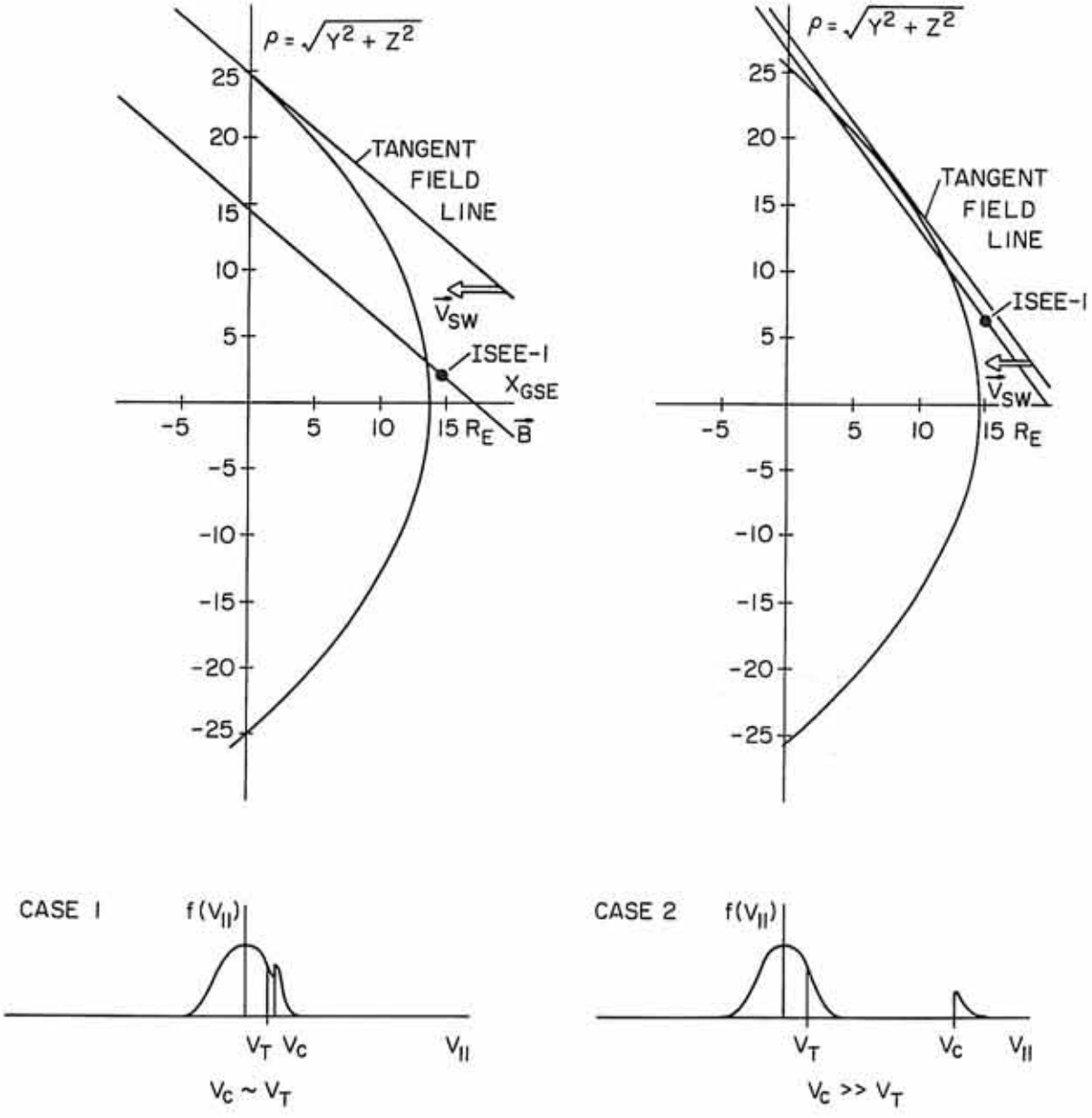

Figure 7

Figure 8 In the upper panels, three reduced one-dimensional distribution obtained from 3 seconds of data spaced 18 seconds apart are illustrated. The middle panel is a plot of high resolution wideband data. The lower panel is a plot of Diff. At 1237:51 - 1237:54, a second peak is observed in the reduced distribution. At 1238:09.2 - 1238:12.2, a plateau is observed in the reduced distribution. At 1238:27.6 -1238:30.6 when ISEE-1 is about 25 R_E downstream of the foreshock boundary, no beam is visible in the reduced distribution. One reason why no beam is visible may be that the beam is varying in velocity space much faster than the 3 seconds used to generate the distribution. Observations of short duration bursts of plasma oscillations at varying frequencies may be evidence of temporal variation of the beam.

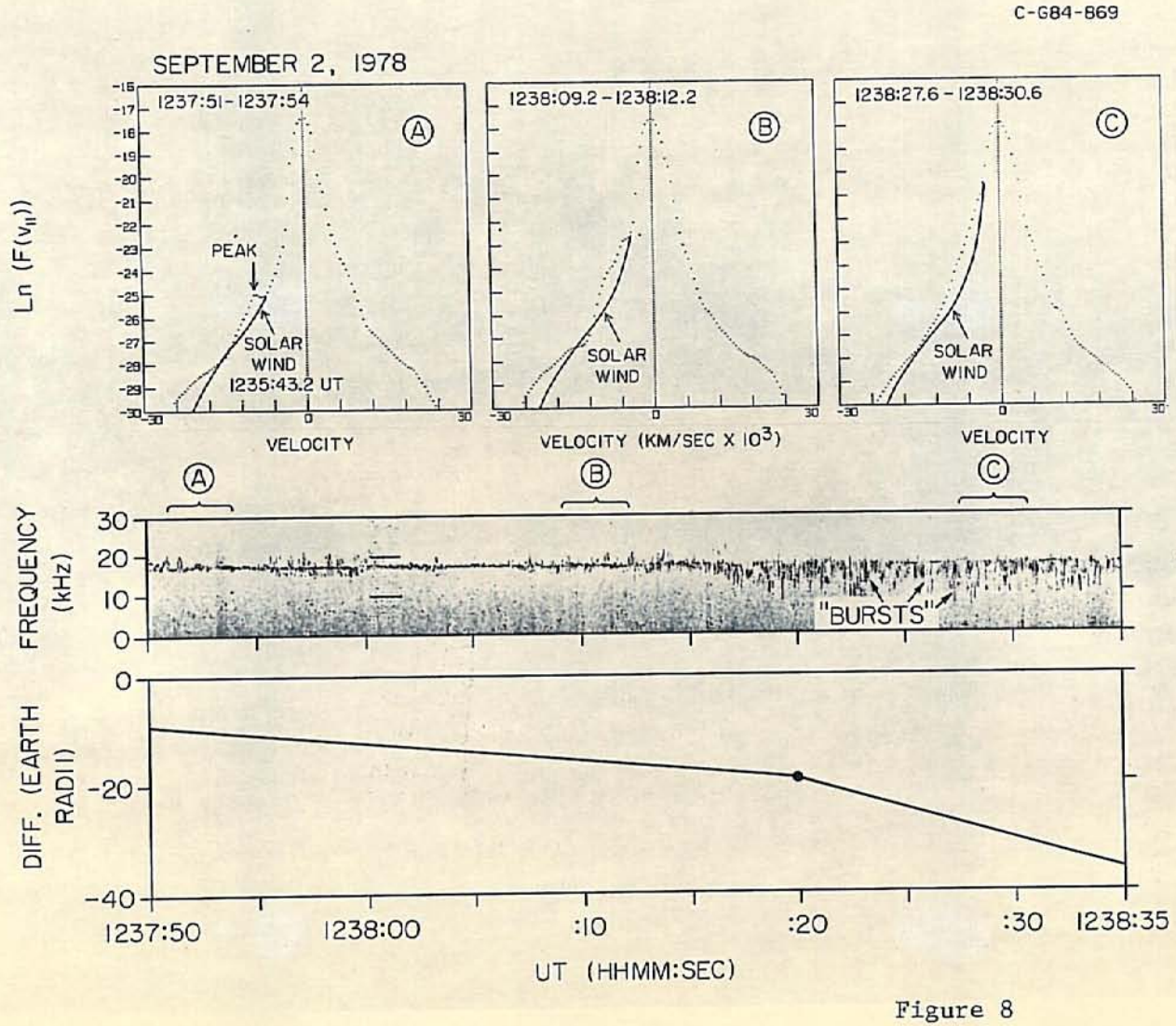
C-G84-869
SEPTEMBER 2, 1978
1237:51-1237:54
1238:09.2-1238:12.2
1238:27.6-1238:30.6
Ln (F(v∥))
PEAK
SOLAR WIND
1235:43.2 UT
VELOCITY
VELOCITY (KM/SEC X 10³)
A
B
C
FREQUENCY (kHz)
"BURSTS"
DIFF. (EARTH RADII)
1237:50
1238:00
:10
:20
:30
1238:35
UT (HHMM:SEC)

Figure 8

Figure 9 Solutions to the linear dispersion relation $D(k,\omega) = 0$ are illustrated. The growth rate or imaginary part of the frequency is plotted versus the real part of the frequency. The number density ratio and beam temperature ratio were fixed at 0.01 and 0.0, respectively. Curves representing $\omega(k)$ for various values of V_b/V_t are illustrated. For specific values of V_b/V_t and n_b/n_o, the observed frequency will be the frequency with the maximum growth rate.

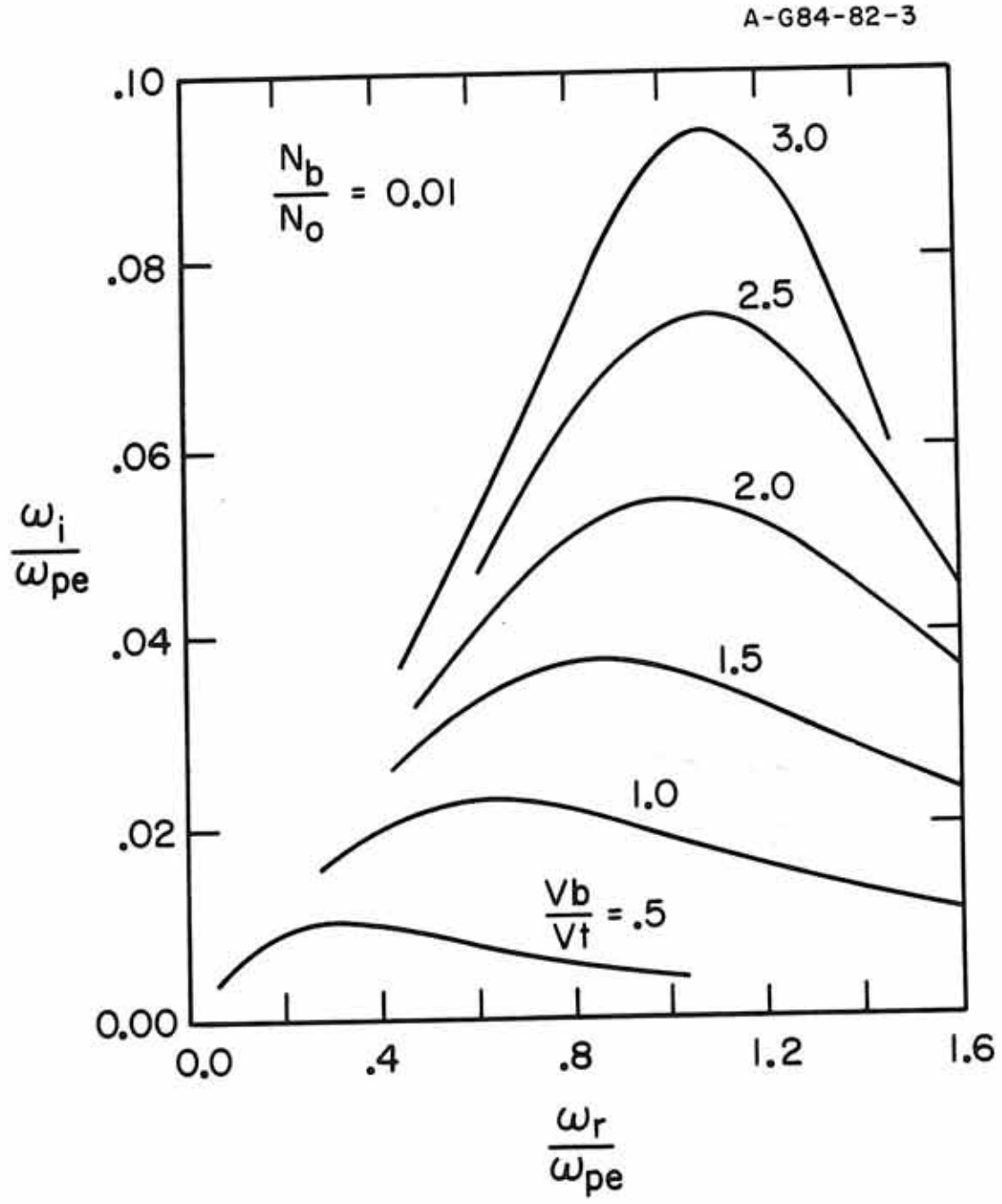
A-G84-82-3
.10
.08
.06
.04
.02
0.00
$\frac{N_b}{N_o}$ = 0.01
3.0
2.5
2.0
1.5
1.0
$\frac{Vb}{Vt}$ = .5
$\frac{\omega_i}{\omega_{pe}}$
0.0
.4
.8
1.2
1.6
$\frac{\omega_r}{\omega_{pe}}$

Figure 9

Figure 10 The frequency of maximum growth determined from solutions of $D(k,\omega) = 0$ is plotted versus V_b/V_t. The number density ratio was fixed at 0.01. Curves for various values of T_b/T_o are illustrated. For $2 < V_b/V_t < 5$, plasma oscillations occur above the plasma frequency. For $V_b/V_t < 2$, plasma oscillations occur below the plasma frequency.

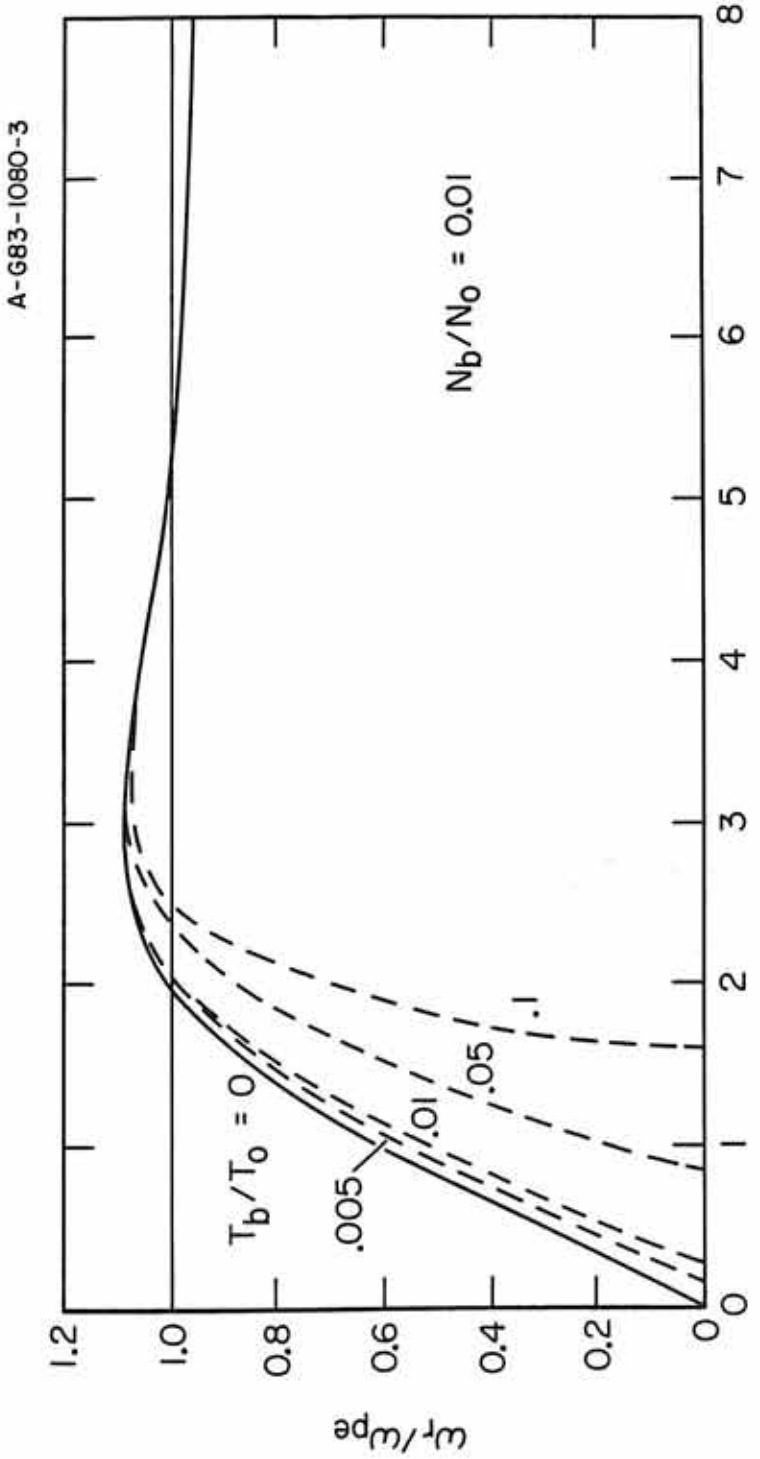
A-G83-1080-3
N_b/N_o = 0.01
T_b/T_o = 0
.005
.01
.05
.1
ω_r/ω_{pe}
V_b/V_t
0
0.2
0.4
0.6
0.8
1.0
1.2
0
1
2
3
4
5
6
7
8

Figure 10

Figure 11 The wave number of maximum growth is plotted versus V_b/V_t. The number density ratio was fixed at 0.01. As V_b/V_t decreases, wavelengths of plasma oscillations decrease. For $V_b/V_t \lesssim 4.5$ wavelengths of plasma oscillations are less than the 215 meter antenna on ISEE-1.

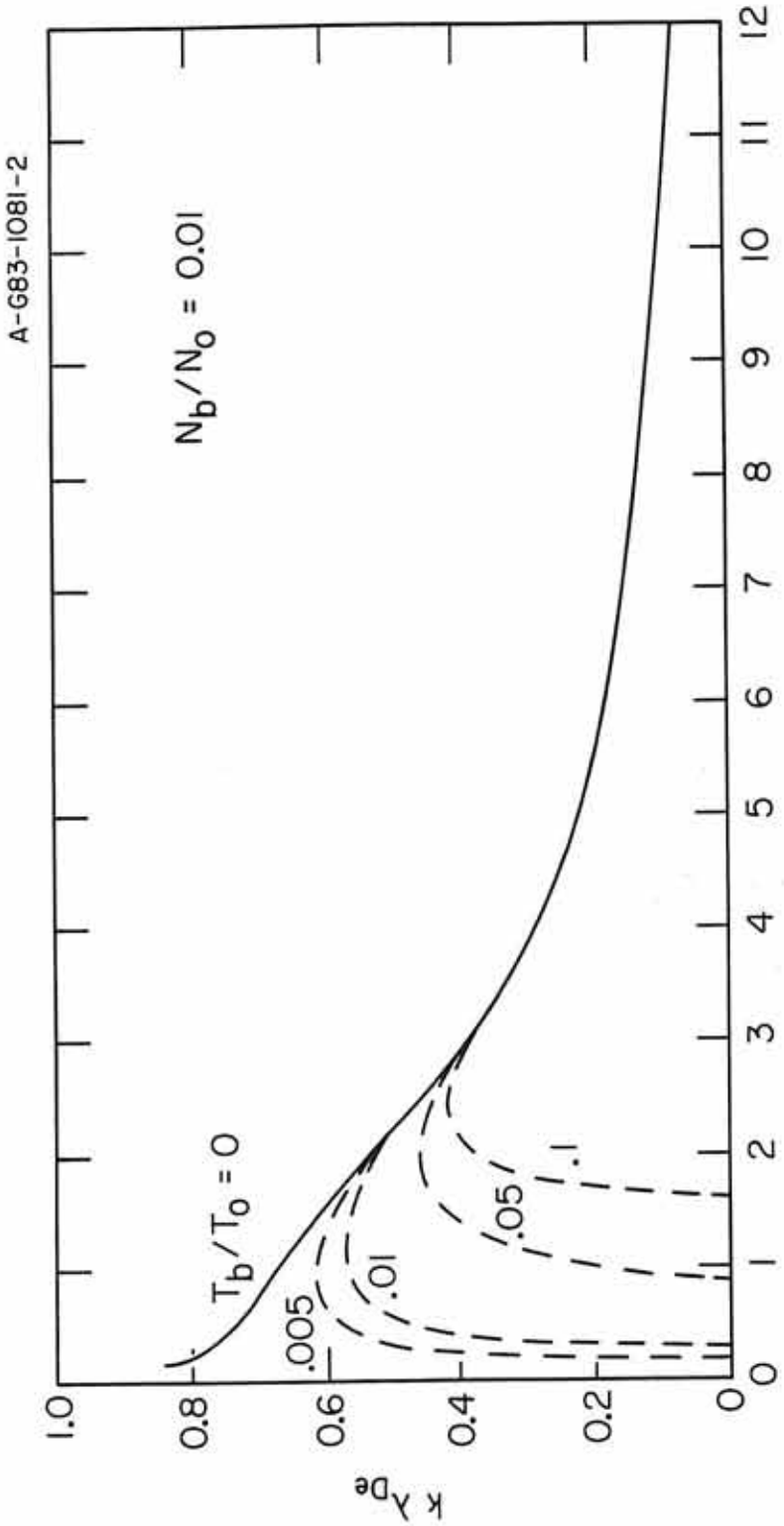
A-G83-1081-2
N_b/N_o = 0.01
T_b/T_o = 0
.005
.01
.05
.1
$k\lambda_{De}$
V_b/V_t
0
0.2
0.4
0.6
0.8
1.0
0
1
2
3
4
5
6
7
8
9
10
11
12

Figure 11

Figure 12 Three examples of model distributions are illustrated. In the first panel, a beam with a velocity of -10,000 km/sec is added to the model solar wind distribution. The resulting distribution is comparable to the observed distribution in the first panel of Figure 8. The next two panels show the effects of averaging beams at different velocities. No positive slope is observed in either distribution. These distributions serve to illustrate that an average of beams at different velocities could account for the lack of a positive slope in the observed reduced distributions in Figure 8.

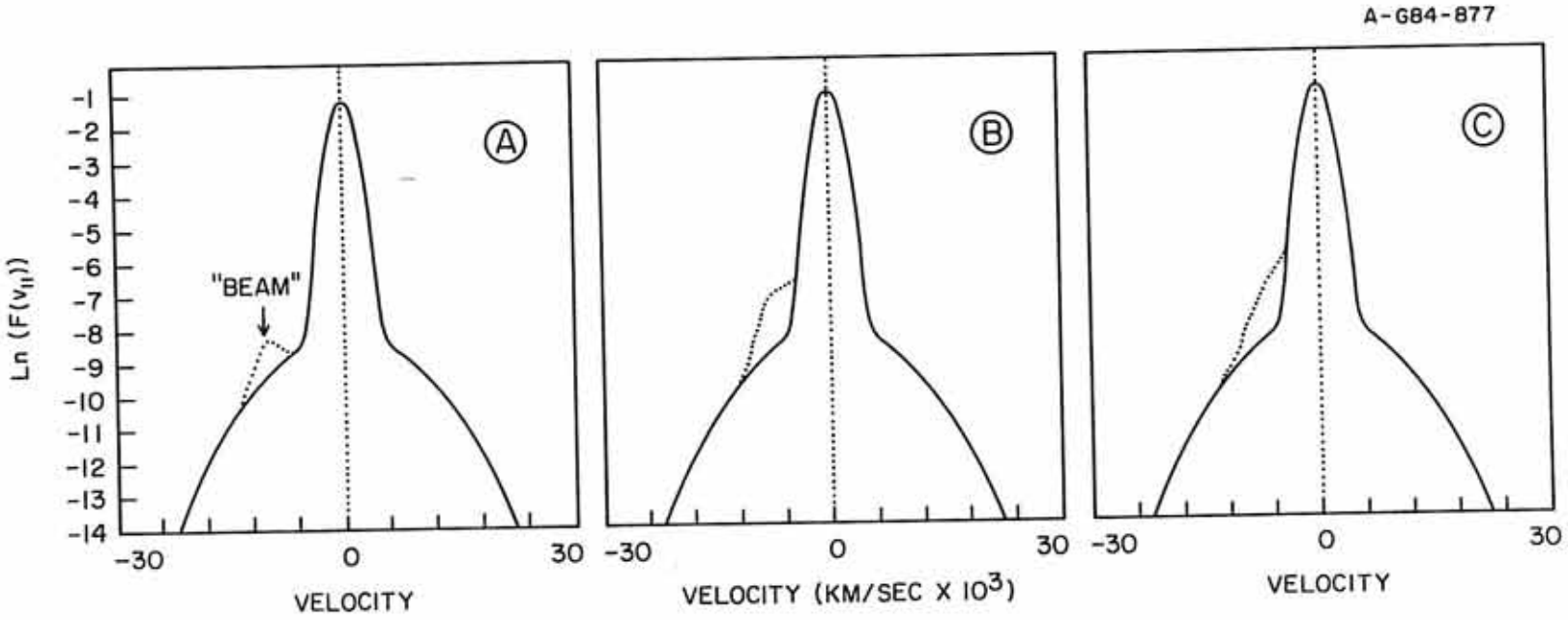
A-G84-877
Ln (F(v||))
-1
-2
-3
-4
-5
-6
-7
-8
-9
-10
-11
-12
-13
-14
"BEAM"
A
B
C
-30
0
30
VELOCITY
VELOCITY (KM/SEC X 10^3)

Figure 12

Figure 13 The definition of Diff depends on whether ISEE-1 is upstream or downstream of the tangent field line. If ISEE-1 is upstream of the tangent field line (left panel), then Diff is defined as the length of the line segment that is perpendicular to both the spacecraft magnetic field line and the bow shock. If ISEE-1 is downstream of the foreshock boundary (right panel) then Diff is defined as the distance from the tangent field line to the spacecraft, measured along the solar wind direction.

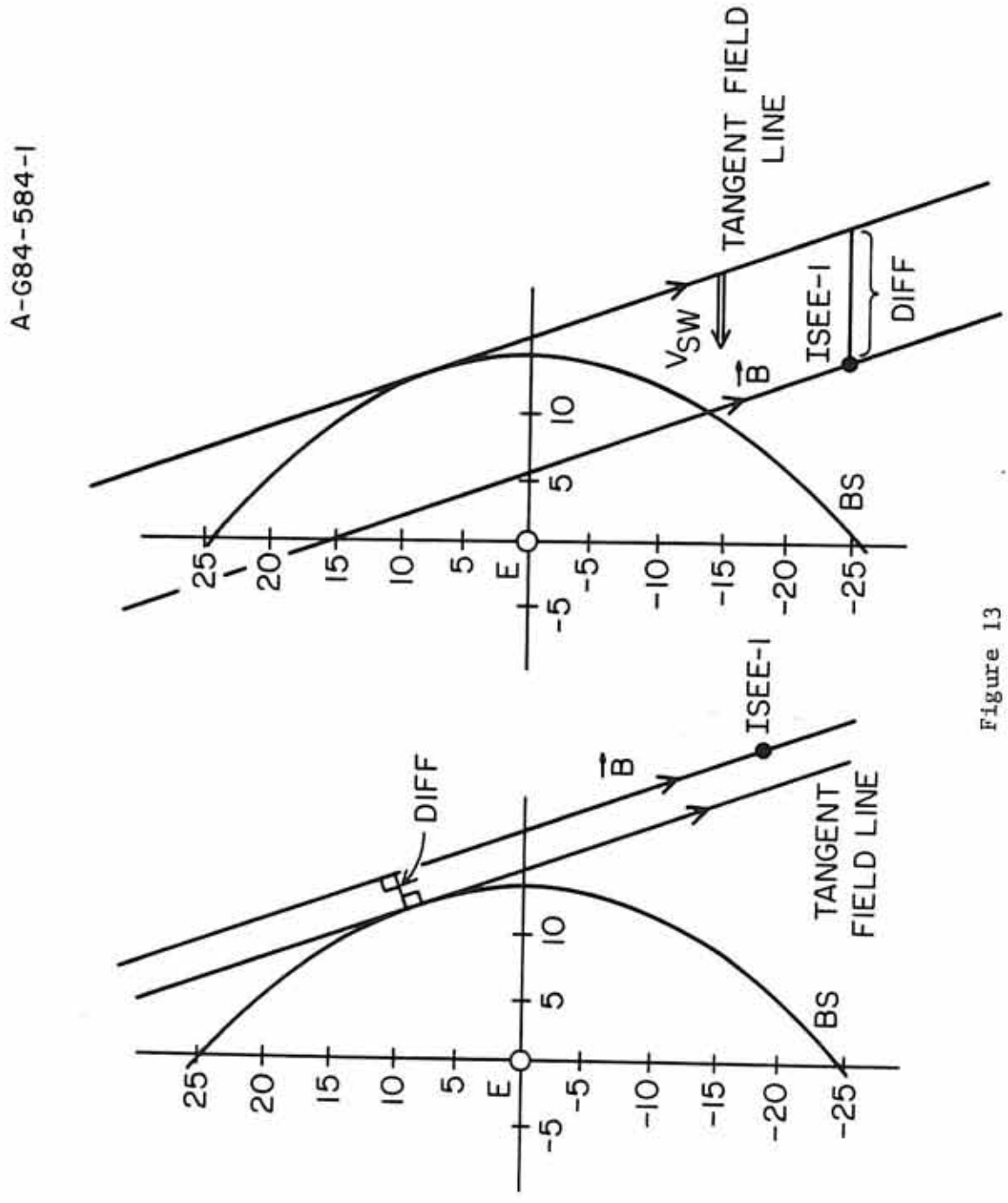
A-G84-584-I
TANGENT FIELD LINE
V_{SW}
$\vec{B}$
ISEE-1
DIFF
BS
E
25
20
15
10
5
-5
-10
-15
-20
-25
10
5
DIFF
$\vec{B}$
ISEE-1
TANGENT FIELD LINE
BS

Figure 13